Non-local Modelling for Fluid Flow Coupled with Heat Transfer by Using Peridynamic Differential Operator

Yan Gao and Selda Oterkus*

Department of Naval Architecture, Ocean and Marine Engineering

University of Strathclyde, 100 Montrose Street, Glasgow, G4 0LZ, United Kingdom

Abstract

The problem of a fluid flow coupled with heat transfer is encountered in many engineering applications. In this study, a non-local model is developed towards such problems by using the peridynamic differential operator. The classical governing equations are reformulated from their differential forms into their integral forms. Furthermore, the non-local model is also cast into the non-dimensional form. Finally, the developed model is applied to simulate pure heat conduction, natural convection, and mixed convection problems. The simulation results are compared with the ones from ANSYS and the published literature. The validity of the proposed model is demonstrated good agreements. The non-local model developed in this study provides an alternative approach for the numerical simulations of the fluid flow coupled with heat transfer problems.

Key Words: peridynamic differential operator, non-local, fluid flow, heat transfer, natural convection, mixed convection

1 INTRODUCTION

The problem of fluid flow coupled with heat transfer has been extensively studied. The convection problem is one of the typical problems within this field. Convection problems are generally divided into two categories, i.e. natural convection and forced convection, depending on the different types of driven forces. Temperature-induced buoyancy forces are responsible for the fluid flow in natural convection. On the other hand, the fluid flow is driven by lid motion in forced convection. A situation where both the natural and the forced convection are comparable is known as mixed convection. The natural and mixed convection problems are encountered in many engineering applications, e.g. the collection of solar energy, food processing, and safety of nuclear reactors et al.[1]. However, the predicting, understanding, and controlling of such complex fluid and thermal systems are challengeable [2]. Due to the

*Corresponding Author: Selda Oterkus, Department of Naval Architecture, Ocean and Marine Engineering, University of Strathclyde. Email: selda.oterkus@strath.ac.uk.

geometrical simplicity, the natural and mixed convection problems within an enclosed cavity have been extensively studied in the literature.

De Vahl Davis [3] provided a benchmark solution for the natural convection in a square cavity with constant temperature boundary conditions. The fluid flow was assumed to be laminar and the Boussinesq approximation was valid. The velocities, temperature, and rates of heat transfer had been obtained for Rayleigh numbers being up to 10^6. According to the experiment study in [4], the fluid flow will switch over to turbulence when the Rayleigh number is larger than 10^6. Later on, the study of the natural convection was extended to the turbulent field for Rayleigh number ranging from 10^6 to 10^{16} [5]. If the natural convection is driven by large temperature differences, the Boussinesq approximation is not applicable because of considerable density variations. Hence, a non-Boussinesq model was proposed by Szewc et al. [6] for such situations. Many numerical simulation methods have been applied for the natural convection simulation, i.e. the finite difference method (FDM) [3], the finite element method (FEM) and the discrete singular convolution (DSC) [7], the smoothed particle hydrodynamics (SPH) [6, 8, 9]. On the other hand, mixed convection in a square enclosed cavity is another benchmark problem. Moallemi and Jang [10] used the Semi-Implicit Method for Pressure-Linked Equations-revised (SIMPLER) [2] algorithm to investigate the effects of the Reynold number and Prandtl number on the flow and the heat transfer. The upper lid has a constant velocity and the bottom wall was heated. Later on, the situation in which the moving top wall was heated and the bottom wall was cooled was discussed by Iwatsu et al. [11]. In their work, the FDM was used to study the effect of the Richardson number, which provided a measure of the importance of natural convection relative to forced convection. FEM with a consistent splitting scheme was used by Wong[12] to simulate the buoyancy-opposing and buoyancy-aiding mixed convection problems. In addition, this benchmark problem has been discussed in extended configurations, e.g. in a two-sided lid-driven cavity [13] or in an inclined driven cavity [14].

The peridynamics (PD) proposed by Silling [15] is a non-local, mesh-free Lagrangian method. In PD, the equation of motion is reformulated from the classical differential form into its integral form. Therefore, no singular stress or strain will be created at discontinuities. The equation will be valid everywhere within the body. This is one of its advantages over the classical numerical simulation methods such as FDM and FEM. It is initially applied in solid mechanics [15-17]. Later on, the peridynamic theory has been applied in other fields [18-32]. However, the application of PD on fluid mechanics has not been extensively studied, only a

few PD fluid models are available in the published literature [33-37]. For the problems of fluid flow coupled with heat transfer, to the authors' knowledge, no PD model is available. Based on the PD concepts, a peridynamic differential operator is developed by Madenci et al. [38]. By using the peridynamic differential operator, the differential equations can be directly converted into their integral form. Therefore, the PD expressions for the classical parameters are avoided. Furthermore, the peridynamic differential operator is applicable for any order derivatives transformation. As a result, the peridynamic differential operator is utilized to convert the governing equations from the differential form into the integral form.

This paper is organized as follows. Firstly, the PD theory and the peridynamic differential operator are briefly reviewed in Section 2. Secondly, the governing equations are reformulated by the peridynamic differential operator in Section 3. Thirdly, the numerical implementation approach is described in Section 4. Subsequently, a pure heat conduction problem, a natural convection problem, and a mixed convection problem are numerically simulated in Section 5. Finally, the conclusions are drawn in Section 6.

2 PERIDYNAMIC DIFFERENTIAL OPERATOR

2.1 Basic Ideas of PD theory

PD is a new formulation of the continuum theory, which uses the integral form of the equation of motion [39]. The PD equations can apply everywhere regardless of discontinuities by omitting the spatial partial derivatives [40]. Therefore, the problems involving discontinuities, which are crucial challenges in classical mechanics, can be solved without any additional criteria.

As shown in Fig. 1, in a body R, each material point is identified by its position $\mathbf{x}\left(x_1, x_2, x_3\right)$. Point $\mathbf{x}$ can interact with other PD material points, $\mathbf{x}'\left(x_1', x_2', x_3'\right)$, within its domain $H_{\mathbf{x}}$. The radius of $H_{\mathbf{x}}$ is called horizon, denoted by δ. Here, $\mathbf{x}$ is the point of interest and $\mathbf{x}'$ is called a family member of $\mathbf{x}$. The relative position between $\mathbf{x}$ and $\mathbf{x}'$ is denoted by $\boldsymbol{\xi}$, i.e. $\mathbf{x}' = \mathbf{x} + \boldsymbol{\xi}$.

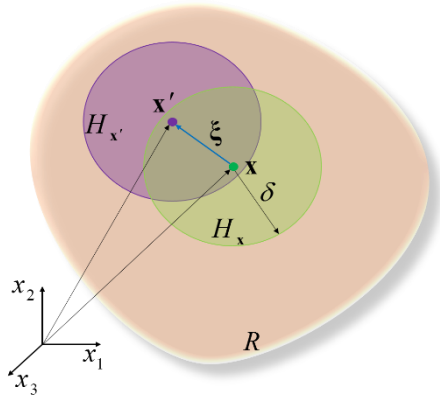

Fig. 1 Interaction of peridynamic central point $\mathbf{x}$ and its family member $\mathbf{x}'$

2.2 Peridynamic differential operator

Based on the PD theory, the peridynamic differential operator is proposed by Madenci et al. [38]. It provides a bridge between the local partial derivatives and the non-local integrals. By using the peridynamic differential operator, the partial differential in any order can directly be converted to its integral form. The peridynamic differential operator is constructed based on Taylor series expansion and orthogonal function properties.

In this study, PD differential operator corresponding to up to second order derivatives in a two-dimensional space is considered. A function f is defined as a scalar field with respect to the variable $\mathbf{x}=(x_1,x_2)$, i.e. $f(\mathbf{x})=f(x_1,x_2)$. The difference between $f(\mathbf{x}+\boldsymbol{\xi})$ and $f(\mathbf{x})$ can be approximated by using Taylor series expansion with ignoring the higher order terms as

$$f(\mathbf{x}+\boldsymbol{\xi})-f(\mathbf{x})=\xi_1\frac{\partial f(\mathbf{x})}{\partial x_1}+\xi_2\frac{\partial f(\mathbf{x})}{\partial x_2}+\frac{1}{2}\xi_1^2\frac{\partial^2 f(\mathbf{x})}{\partial x_1^2}+\frac{1}{2}\xi_2^2\frac{\partial^2 f(\mathbf{x})}{\partial x_2^2}+\xi_1\xi_2\frac{\partial^2 f(\mathbf{x})}{\partial x_1\partial x_2} \quad (1)$$

or [38]

$$f(\mathbf{x}+\boldsymbol{\xi})-f(\mathbf{x})=\sum_{n_1=0}^{2}\sum_{n_2=0}^{2-n_1}\frac{1}{n_1!n_2!}\xi_1^{n_1}\xi_2^{n_2}\frac{\partial^{n_1+n_2}f(\mathbf{x})}{\partial x_1^{n_1}\partial x_2^{n_2}},\ 0<n_1+n_2\le 2 \quad (2)$$

where n_1 and n_2 represent the differential order with respect to x_1 and x_2. The term $\boldsymbol{\xi}$ is represented as

$$\boldsymbol{\xi}=\xi_1\mathbf{e}_1+\xi_2\mathbf{e}_2 \quad (3)$$

where $\mathbf{e}_1$ and $\mathbf{e}_2$ represent the unit vectors in the x_1 and x_2 directions. The components ξ_1 and ξ_2 are evaluated as

$$\xi_1 = x_1' - x_1 \tag{4a}$$

$$\xi_2 = x_2' - x_2 \tag{4b}$$

The peridynamic differential operator, $g^{p_1 p_2}(\boldsymbol{\xi})$, corresponds to the term $\partial^{p_1+p_2} f(\mathbf{x}) / \partial x_1^{p_1} \partial x_2^{p_2}$ with the integer variable constraint $0 < p_1 + p_2 \le 2$ [38]. For example, $g^{10}(\boldsymbol{\xi})$ is set to correspond to $\partial^{1+0} f(\mathbf{x}) / \partial x_1^1 \partial x_2^0$. The peridynamic differential operator possess the orthogonal property as [38]

$$\int_{H_\mathbf{x}} \xi_1^{n_1} \xi_2^{n_2} g^{p_1 p_2}(\boldsymbol{\xi}) \mathrm{d}V' = n_1! n_2! \delta_{n_1 p_1} \delta_{n_2 p_2} \tag{5}$$

where

$$\delta_{n_i p_i} = \begin{cases} 0, \text{ if } n_i \ne p_i \\ 1, \text{ if } n_i = p_i \end{cases} \tag{6}$$

with $i = 1, 2$. Multiplying $g^{p_1 p_2}(\boldsymbol{\xi})$ on both sides of Eq. (2) and integrating over the horizon domain, $H_\mathbf{x}$, results in [38]

$$\begin{aligned} &\int_{H_\mathbf{x}} \left(f(\mathbf{x}+\boldsymbol{\xi}) - f(\mathbf{x}) \right) g^{p_1 p_2}(\boldsymbol{\xi}) \mathrm{d}V' \\ &= \sum_{n_1=0}^{2} \sum_{n_2=0}^{2-n_1} \frac{1}{n_1! n_2!} \int_{H_\mathbf{x}} \frac{\partial^{n_1+n_2} f(\mathbf{x})}{\partial x_1^{n_1} \partial x_2^{n_2}} \xi_1^{n_1} \xi_2^{n_2} g^{p_1 p_2}(\boldsymbol{\xi}) \mathrm{d}V', \; 0 < n_1 + n_2 \le 2 \end{aligned} \tag{7}$$

By using the orthogonal property described in Eq.(5), Eq.(7) becomes

$$\begin{aligned} &\int_{H_\mathbf{x}} \left(f(\mathbf{x}+\boldsymbol{\xi}) - f(\mathbf{x}) \right) g^{p_1 p_2}(\boldsymbol{\xi}) \mathrm{d}V' \\ &= \frac{1}{p_1! p_2!} \int_{H_\mathbf{x}} \frac{\partial^{p_1+p_2} f(\mathbf{x})}{\partial x_1^{p_1} \partial x_2^{p_2}} \xi_1^{p_1} \xi_2^{p_2} g^{p_1 p_2}(\boldsymbol{\xi}) \mathrm{d}V' \\ &= \frac{\partial^{p_1+p_2} f(\mathbf{x})}{\partial x_1^{p_1} \partial x_2^{p_2}} \end{aligned} \tag{8}$$

Eq.(8) can be rewritten as [38]

$$\begin{Bmatrix} \dfrac{\partial f(\mathbf{x})}{\partial x_1} \\ \dfrac{\partial f(\mathbf{x})}{\partial x_2} \\ \dfrac{\partial^2 f(\mathbf{x})}{\partial x_1^2} \\ \dfrac{\partial^2 f(\mathbf{x})}{\partial x_2^2} \\ \dfrac{\partial^2 f(\mathbf{x})}{\partial x_1 \partial x_2} \end{Bmatrix} = \int_{H_{\mathbf{x}}} \left(f(\mathbf{x}+\boldsymbol{\xi}) - f(\mathbf{x}) \right) \begin{Bmatrix} g^{10}(\boldsymbol{\xi}) \\ g^{01}(\boldsymbol{\xi}) \\ g^{20}(\boldsymbol{\xi}) \\ g^{02}(\boldsymbol{\xi}) \\ g^{11}(\boldsymbol{\xi}) \end{Bmatrix} \mathrm{d}V' \tag{9}$$

The spatial differentials of $f(\mathbf{x})$ can be approximated by using the integrations as provided Eq.(9).

The PD differential operators, $g^{p_1 p_2}(\boldsymbol{\xi})$, are chosen as [38]

$$for\ g^{10}(\boldsymbol{\xi}):\ g^{10}(\boldsymbol{\xi}) = \left(a_{10}^{10}\right) w\xi_1 + \left(a_{01}^{10}\right) w\xi_2 + \left(a_{20}^{10}\right) w\xi_1^2 + \left(a_{02}^{10}\right) w\xi_2^2 + \left(a_{11}^{10}\right) w\xi_1\xi_2 \tag{10a}$$

$$for\ g^{01}(\boldsymbol{\xi}):\ g^{01}(\boldsymbol{\xi}) = \left(a_{10}^{01}\right) w\xi_1 + \left(a_{01}^{01}\right) w\xi_2 + \left(a_{20}^{01}\right) w\xi_1^2 + \left(a_{02}^{01}\right) w\xi_2^2 + \left(a_{11}^{01}\right) w\xi_1\xi_2 \tag{10b}$$

$$for\ g^{20}(\boldsymbol{\xi}):\ g^{20}(\boldsymbol{\xi}) = \left(a_{10}^{20}\right) w\xi_1 + \left(a_{01}^{20}\right) w\xi_2 + \left(a_{20}^{20}\right) w\xi_1^2 + \left(a_{02}^{20}\right) w\xi_2^2 + \left(a_{11}^{20}\right) w\xi_1\xi_2 \tag{10c}$$

$$for\ g^{02}(\boldsymbol{\xi}):\ g^{02}(\boldsymbol{\xi}) = \left(a_{10}^{02}\right) w\xi_1 + \left(a_{01}^{02}\right) w\xi_2 + \left(a_{20}^{02}\right) w\xi_1^2 + \left(a_{02}^{02}\right) w\xi_2^2 + \left(a_{11}^{02}\right) w\xi_1\xi_2 \tag{10d}$$

$$for\ g^{11}(\boldsymbol{\xi}):\ g^{11}(\boldsymbol{\xi}) = \left(a_{10}^{11}\right) w\xi_1 + \left(a_{01}^{11}\right) w\xi_2 + \left(a_{20}^{11}\right) w\xi_1^2 + \left(a_{02}^{11}\right) w\xi_2^2 + \left(a_{11}^{11}\right) w\xi_1\xi_2 \tag{10e}$$

Eq. (10) can also be written in a matrix form as [38]

$$\begin{Bmatrix} g^{10}(\boldsymbol{\xi}) \\ g^{01}(\boldsymbol{\xi}) \\ g^{20}(\boldsymbol{\xi}) \\ g^{02}(\boldsymbol{\xi}) \\ g^{11}(\boldsymbol{\xi}) \end{Bmatrix} = \begin{bmatrix} a_{10}^{10} & a_{01}^{10} & a_{20}^{10} & a_{02}^{10} & a_{11}^{10} \\ a_{10}^{01} & a_{01}^{01} & a_{20}^{01} & a_{02}^{01} & a_{11}^{01} \\ a_{10}^{20} & a_{01}^{20} & a_{20}^{20} & a_{02}^{20} & a_{11}^{20} \\ a_{10}^{02} & a_{01}^{02} & a_{20}^{02} & a_{02}^{02} & a_{11}^{02} \\ a_{10}^{11} & a_{01}^{11} & a_{20}^{11} & a_{02}^{11} & a_{11}^{11} \end{bmatrix} \begin{Bmatrix} w\xi_1 \\ w\xi_2 \\ w\xi_1^2 \\ w\xi_2^2 \\ w\xi_1\xi_2 \end{Bmatrix} \tag{11}$$

where $a_{q_1 q_2}^{p_1 p_2}$ with $0 < q_1 + q_2 \le 2$ represents the unknown coefficient. In Eq.(10) and Eq.(11), w is the weight function defined as [38]

$$w = e^{-\left(2|\xi|/\delta\right)^2} \tag{12}$$

The unknown coefficients in Eq. (11) can be obtained by using the orthogonality condition in Eq. (5) for each differential operator. For example, the unknown coefficients in Eq. (10a) are obtained from following orthogonality conditions:

$$\begin{aligned}&\left(a_{10}^{10}\right)\int_{H_{\mathbf{x}}} w\xi_1^2 \mathrm{d}V' + \left(a_{01}^{10}\right)\int_{H_{\mathbf{x}}} w\xi_1\xi_2 \mathrm{d}V' + \left(a_{20}^{10}\right)\int_{H_{\mathbf{x}}} w\xi_1^3 \mathrm{d}V' \\ &+\left(a_{02}^{10}\right)\int_{H_{\mathbf{x}}} w\xi_1\xi_2^2 \mathrm{d}V' + \left(a_{11}^{10}\right)\int_{H_{\mathbf{x}}} w\xi_1^2\xi_2 \mathrm{d}V' = 1\end{aligned} \tag{13a}$$

$$\begin{aligned}&\left(a_{10}^{10}\right)\int_{H_{\mathbf{x}}} w\xi_1\xi_2 \mathrm{d}V' + \left(a_{01}^{10}\right)\int_{H_{\mathbf{x}}} w\xi_2^2 \mathrm{d}V' + \left(a_{20}^{10}\right)\int_{H_{\mathbf{x}}} w\xi_1^2\xi_2 \mathrm{d}V' \\ &+\left(a_{02}^{10}\right)\int_{H_{\mathbf{x}}} w\xi_2^3 \mathrm{d}V' + \left(a_{11}^{10}\right)\int_{H_{\mathbf{x}}} w\xi_1\xi_2^2 \mathrm{d}V' = 0\end{aligned} \tag{13b}$$

$$\begin{aligned}&\left(a_{10}^{10}\right)\int_{H_{\mathbf{x}}} w\xi_1^3 \mathrm{d}V' + \left(a_{01}^{10}\right)\int_{H_{\mathbf{x}}} w\xi_1^2\xi_2 \mathrm{d}V' + \left(a_{20}^{10}\right)\int_{H_{\mathbf{x}}} w\xi_1^4 \mathrm{d}V' \\ &+\left(a_{02}^{10}\right)\int_{H_{\mathbf{x}}} w\xi_1^2\xi_2^2 \mathrm{d}V' + \left(a_{11}^{10}\right)\int_{H_{\mathbf{x}}} w\xi_1^3\xi_2 \mathrm{d}V' = 0\end{aligned} \tag{13c}$$

$$\begin{aligned}&\left(a_{10}^{10}\right)\int_{H_{\mathbf{x}}} w\xi_1\xi_2^2 \mathrm{d}V' + \left(a_{01}^{10}\right)\int_{H_{\mathbf{x}}} w\xi_2^3 \mathrm{d}V' + \left(a_{20}^{10}\right)\int_{H_{\mathbf{x}}} w\xi_1^2\xi_2^2 \mathrm{d}V' \\ &+\left(a_{02}^{10}\right)\int_{H_{\mathbf{x}}} w\xi_2^4 \mathrm{d}V' + \left(a_{11}^{10}\right)\int_{H_{\mathbf{x}}} w\xi_1\xi_2^3 \mathrm{d}V' = 0\end{aligned} \tag{13d}$$

$$\begin{aligned}&\left(a_{10}^{10}\right)\int_{H_{\mathbf{x}}} w\xi_1^2\xi_2 \mathrm{d}V' + \left(a_{01}^{10}\right)\int_{H_{\mathbf{x}}} w\xi_1\xi_2^2 \mathrm{d}V' + \left(a_{20}^{10}\right)\int_{H_{\mathbf{x}}} w\xi_1^3\xi_2 \mathrm{d}V' \\ &+\left(a_{02}^{10}\right)\int_{H_{\mathbf{x}}} w\xi_1\xi_2^3 \mathrm{d}V' + \left(a_{11}^{10}\right)\int_{H_{\mathbf{x}}} w\xi_1^2\xi_2^2 \mathrm{d}V' = 0\end{aligned} \tag{13e}$$

Similarly, the unknown coefficients in Eq.(10b-e) can be obtained by using the orthogonality condition provided in Eq.(5). Thus, the unknown coefficient matrix is obtained by the following relation

$$\mathbf{Aa} = \mathbf{b} \tag{14}$$

where

$$\mathbf{A} = \int_{H_{\mathbf{x}}} w \begin{bmatrix} \xi_1^2 & \xi_1\xi_2 & \xi_1^3 & \xi_1\xi_2^2 & \xi_1^2\xi_2 \\ \xi_1\xi_2 & \xi_2^2 & \xi_1^2\xi_2 & \xi_2^3 & \xi_1\xi_2^2 \\ \xi_1^3 & \xi_1^2\xi_2 & \xi_1^4 & \xi_1^2\xi_2^2 & \xi_1^3\xi_2 \\ \xi_1\xi_2^2 & \xi_2^3 & \xi_1^2\xi_2^2 & \xi_2^4 & \xi_1\xi_2^3 \\ \xi_1^2\xi_2 & \xi_1\xi_2^2 & \xi_1^3\xi_2 & \xi_1\xi_2^3 & \xi_1^2\xi_2^2 \end{bmatrix} \mathrm{d}V' \tag{15a}$$

$$\mathbf{a}=\begin{bmatrix} a_{10}^{10} & a_{10}^{01} & a_{10}^{20} & a_{10}^{02} & a_{10}^{11} \\ a_{01}^{10} & a_{01}^{01} & a_{01}^{20} & a_{01}^{02} & a_{01}^{11} \\ a_{20}^{10} & a_{20}^{01} & a_{20}^{20} & a_{20}^{02} & a_{20}^{11} \\ a_{02}^{10} & a_{02}^{01} & a_{02}^{20} & a_{02}^{02} & a_{02}^{11} \\ a_{11}^{10} & a_{11}^{01} & a_{11}^{20} & a_{11}^{02} & a_{11}^{11} \end{bmatrix} \tag{15b}$$

$$\mathbf{b}=\begin{bmatrix} 1 & 0 & 0 & 0 & 0 \\ 0 & 1 & 0 & 0 & 0 \\ 0 & 0 & 2 & 0 & 0 \\ 0 & 0 & 0 & 2 & 0 \\ 0 & 0 & 0 & 0 & 1 \end{bmatrix} \tag{15c}$$

Finally, PD differential operators can be obtained by substituting Eq.(15b) into Eq.(11).

3 NON-LOCAL GOVERNING EQUATIONS

In this section, by using the peridyamic differential operator, the governing equations which describe the fluid flow coupled with heat transfer are reformulated into non-local form. The fluid flow is assumed as Newtonian fluid incompressible, viscous, laminar, two-dimensional, heat conducting flow.

3.1 Conservation of Mass

The local form of conservation of mass is defined as [41]

$$\frac{\partial \rho}{\partial t}+v_1\frac{\partial \rho}{\partial x_1}+v_2\frac{\partial \rho}{\partial x_2}=-\rho\left(\frac{\partial v_1}{\partial x_1}+\frac{\partial v_2}{\partial x_2}\right) \tag{16}$$

where left-hand side represents the material derivative of density. The terms v_1 and v_2 represent velocity components of $\mathbf{v}$ in x_1 and x_2 directions respectively. The partial spatial derivatives in Eq.(16) can be converted into their non-local form by applying Eq. (9) as

$$\frac{\partial v_1(\mathbf{x})}{\partial x_1}=\int_{H_\mathbf{x}}\left(v_1(\mathbf{x}')-v_1(\mathbf{x})\right)\mathrm{g}^{10}(\boldsymbol{\xi})\,\mathrm{d}V' \tag{17a}$$

$$\frac{\partial v_2(\mathbf{x})}{\partial x_2}=\int_{H_\mathbf{x}}\left(v_2(\mathbf{x}')-v_2(\mathbf{x})\right)\mathrm{g}^{01}(\boldsymbol{\xi})\,\mathrm{d}V' \tag{17b}$$

$$\frac{\partial \rho(\mathbf{x})}{\partial x_1}=\int_{H_\mathbf{x}}\left(\rho(\mathbf{x}')-\rho(\mathbf{x})\right)\mathrm{g}^{10}(\boldsymbol{\xi})\,\mathrm{d}V' \tag{17c}$$

$$\frac{\partial \rho(\mathbf{x})}{\partial x_2} = \int_{H_\mathbf{x}} \left(\rho(\mathbf{x}') - \rho(\mathbf{x})\right) \mathrm{g}^{01}(\boldsymbol{\xi}) \mathrm{d}V' \tag{17d}$$

By substituting Eq. (17) into Eq.(16), the non-local form of the conservation equation of mass can be evaluated as

$$\begin{aligned}\frac{\partial \rho(\mathbf{x})}{\partial t} = &-\rho(\mathbf{x}) \int_{H_\mathbf{x}} \left(\left(v_1(\mathbf{x}') - v_1(\mathbf{x})\right) \mathrm{g}^{10}(\boldsymbol{\xi}) + \left(v_2(\mathbf{x}') - v_2(\mathbf{x})\right) \mathrm{g}^{01}(\boldsymbol{\xi})\right) \mathrm{d}V' \\ &- \int_{H_\mathbf{x}} \left(\rho(\mathbf{x}') - \rho(\mathbf{x})\right)\left(v_1(\mathbf{x}) \mathrm{g}^{10}(\boldsymbol{\xi}) + v_2(\mathbf{x}) \mathrm{g}^{01}(\boldsymbol{\xi})\right) \mathrm{d}V'\end{aligned} \tag{18}$$

For an incompressible flow, the conservation of mass becomes

$$\frac{\partial v_1}{\partial x_1} + \frac{\partial v_2}{\partial x_2} = 0 \tag{19}$$

However, the time step size needs to be extremely small in numerical simulations [42-44]. As a result, the incompressible fluid flow is simulated as weakly compressible fluid flow [43, 44]. The density is still updated according to Eq.(18).

3.2 Constitutive Equation

For a Newtonian fluid incompressible two-dimensional flow, the stress tensor, $\boldsymbol{\sigma}$ is defined as [41]

$$\boldsymbol{\sigma} = -p\mathbf{I} + \mu\left(\nabla \otimes \mathbf{v} + (\nabla \otimes \mathbf{v})^T\right) \tag{20}$$

where $\mathbf{I}$ is a unit second order tensor, p is pressure, and μ is dynamic viscosity. The stress tensor in Eq.(20) can also be written as [41]

$$\boldsymbol{\sigma} = -p\mathbf{I} + \begin{bmatrix} 2\mu \dfrac{\partial v_1}{\partial x_1} & \mu\left(\dfrac{\partial v_1}{\partial x_2} + \dfrac{\partial v_2}{\partial x_1}\right) \\ \mu\left(\dfrac{\partial v_1}{\partial x_2} + \dfrac{\partial v_2}{\partial x_1}\right) & 2\mu \dfrac{\partial v_2}{\partial x_2} \end{bmatrix} \tag{21}$$

By using Eq. (9), the non-local form of the velocity derivatives can be expressed as

$$\frac{\partial v_i}{\partial x_1} = \int_{H_\mathbf{x}} \left(v_i(\mathbf{x}') - v_i(\mathbf{x})\right) \mathrm{g}^{10}(\boldsymbol{\xi}) \mathrm{d}V' \tag{22a}$$

$$\frac{\partial v_i}{\partial x_2} = \int_{H_{\mathbf{x}}} \left(v_i\left(\mathbf{x}'\right) - v_i\left(\mathbf{x}\right) \right) \mathrm{g}^{01}\left(\boldsymbol{\xi}\right) \mathrm{d}V' \tag{22b}$$

with $i = 1,2$. By substituting Eq. (22) into Eq.(21), the non-local form of the stress tensor can be evaluated as

$$\boldsymbol{\sigma} = -p\mathbf{I} + \mu \int_{H_{\mathbf{x}}} \begin{bmatrix} 2\left(v_1\left(\mathbf{x}'\right) - v_1\left(\mathbf{x}\right)\right)\mathrm{g}^{10}\left(\boldsymbol{\xi}\right) & \begin{pmatrix} \left(v_1\left(\mathbf{x}'\right) - v_1\left(\mathbf{x}\right)\right)\mathrm{g}^{01}\left(\boldsymbol{\xi}\right) + \\ \left(v_2\left(\mathbf{x}'\right) - v_2\left(\mathbf{x}\right)\right)\mathrm{g}^{10}\left(\boldsymbol{\xi}\right) \end{pmatrix} \\ \begin{pmatrix} \left(v_1\left(\mathbf{x}'\right) - v_1\left(\mathbf{x}\right)\right)\mathrm{g}^{01}\left(\boldsymbol{\xi}\right) + \\ \left(v_2\left(\mathbf{x}'\right) - v_2\left(\mathbf{x}\right)\right)\mathrm{g}^{10}\left(\boldsymbol{\xi}\right) \end{pmatrix} & 2\left(v_2\left(\mathbf{x}'\right) - v_2\left(\mathbf{x}\right)\right)\mathrm{g}^{01}\left(\boldsymbol{\xi}\right) \end{bmatrix} \mathrm{d}V' \tag{23}$$

The pressure can be calculated according to the equation of state as [45]

$$p = \frac{\rho_0 c_s^2}{\gamma}\left(\left(\frac{\rho}{\rho_0} \right)^{\gamma} - 1 \right) \tag{24}$$

where ρ_0 is the initial density, c_s is the speed of sound, and γ is the ratio of specific heat capacity with $\gamma = 1$ for gas in the present work. In this study, the speed of sound is assumed as 10 times of the maximum fluid velocity.

3.3 Conservation of Momentum

The local form of the conservation of momentum is defined as [41]

$$\rho\left(\frac{\partial \mathbf{v}}{\partial t} + \mathbf{v} \cdot \nabla \mathbf{v} \right) = \nabla \bullet \boldsymbol{\sigma} + \rho \mathbf{g} \tag{25}$$

where $\mathbf{g}$ represents the body force due to gravity. By using the definition of stress tensor in Eq. (21) and the incompressible flow constraint in Eq.(19), the divergence of the stress in local form can be calculated as [41]

$$\nabla \bullet \boldsymbol{\sigma} = \begin{bmatrix} -\frac{\partial p}{\partial x_1} + \mu\left(\frac{\partial^2 v_1}{\partial x_1^2} + \frac{\partial^2 v_1}{\partial x_2^2} \right) + 2\frac{\partial \mu}{\partial x_1}\frac{\partial v_1}{\partial x_1} + \frac{\partial \mu}{\partial x_2}\left(\frac{\partial v_1}{\partial x_2} + \frac{\partial v_2}{\partial x_1} \right) \\ -\frac{\partial p}{\partial x_2} + \mu\left(\frac{\partial^2 v_2}{\partial x_1^2} + \frac{\partial^2 v_2}{\partial x_2^2} \right) + 2\frac{\partial \mu}{\partial x_2}\frac{\partial v_2}{\partial x_2} + \frac{\partial \mu}{\partial x_1}\left(\frac{\partial v_1}{\partial x_2} + \frac{\partial v_2}{\partial x_1} \right) \end{bmatrix} \tag{26}$$

The viscosity μ in general is a function of the thermodynamic state of fluid [41]. Therefore viscosity, $\mu(\mathbf{x})$, is not assumed constant in Eq. (26).

By using Eq.(9), the non-local form of the spatial differentials in Eq. (26) can be expressed as

$$\frac{\partial \mu(\mathbf{x})}{\partial x_1} = \int_{H_\mathbf{x}} \left(\mu(\mathbf{x}') - \mu(\mathbf{x})\right) g^{10}(\boldsymbol{\xi}) \mathrm{d}V'; \frac{\partial \mu(\mathbf{x})}{\partial x_2} = \int_{H_\mathbf{x}} \left(\mu(\mathbf{x}') - \mu(\mathbf{x})\right) g^{01}(\boldsymbol{\xi}) \mathrm{d}V' \quad (27a)$$

$$\frac{\partial p(\mathbf{x})}{\partial x_1} = \int_{H_\mathbf{x}} \left(p(\mathbf{x}') - p(\mathbf{x})\right) \mathrm{g}^{10}(\boldsymbol{\xi}) \mathrm{d}V'; \frac{\partial p(\mathbf{x})}{\partial x_2} = \int_{H_\mathbf{x}} \left(p(\mathbf{x}') - p(\mathbf{x})\right) \mathrm{g}^{01}(\boldsymbol{\xi}) \mathrm{d}V' \quad (27b)$$

$$\frac{\partial^2 v_i(\mathbf{x})}{\partial x_1^2} = \int_{H_\mathbf{x}} \left(v_i(\mathbf{x}') - v_i(\mathbf{x})\right) \mathrm{g}^{20}(\boldsymbol{\xi}) \mathrm{d}V'; \frac{\partial^2 v_i(\mathbf{x})}{\partial x_2^2} = \int_{H_\mathbf{x}} \left(v_i(\mathbf{x}') - v_i(\mathbf{x})\right) \mathrm{g}^{02}(\boldsymbol{\xi}) \mathrm{d}V' \quad (27c)$$

where $i = 1,2$. Subsequently, by substituting Eq. (17a-b) and Eq. (27) into Eq.(26), the non-local form of the divergence of the stress tensor can be calculated as

$$\begin{aligned}
\nabla \bullet \boldsymbol{\sigma} = &-\begin{bmatrix} \int_{H_\mathbf{x}} \left(p(\mathbf{x}') - p(\mathbf{x})\right) \mathrm{g}^{10}(\boldsymbol{\xi}) \mathrm{d}V' \\ \int_{H_\mathbf{x}} \left(p(\mathbf{x}') - p(\mathbf{x})\right) \mathrm{g}^{01}(\boldsymbol{\xi}) \mathrm{d}V' \end{bmatrix} + \mu \begin{bmatrix} \int_{H_\mathbf{x}} \left(v_1(\mathbf{x}') - v_1(\mathbf{x})\right)\left(\mathrm{g}^{20}(\boldsymbol{\xi}) + \mathrm{g}^{02}(\boldsymbol{\xi})\right) \mathrm{d}V' \\ \int_{H_\mathbf{x}} \left(v_2(\mathbf{x}') - v_2(\mathbf{x})\right)\left(\mathrm{g}^{20}(\boldsymbol{\xi}) + \mathrm{g}^{02}(\boldsymbol{\xi})\right) \mathrm{d}V' \end{bmatrix} \\
&+ \begin{bmatrix} 2\left(\int_{H_\mathbf{x}} \left(\mu(\mathbf{x}') - \mu(\mathbf{x})\right) \mathrm{g}^{10}(\boldsymbol{\xi}) \mathrm{d}V'\right)\left(\int_{H_\mathbf{x}} \left(v_1(\mathbf{x}') - v_1(\mathbf{x})\right) \mathrm{g}^{10}(\boldsymbol{\xi}) \mathrm{d}V'\right) \\ 2\left(\int_{H_\mathbf{x}} \left(\mu(\mathbf{x}') - \mu(\mathbf{x})\right) \mathrm{g}^{01}(\boldsymbol{\xi}) \mathrm{d}V'\right)\left(\int_{H_\mathbf{x}} \left(v_2(\mathbf{x}') - v_2(\mathbf{x})\right) \mathrm{g}^{01}(\boldsymbol{\xi}) \mathrm{d}V'\right) \end{bmatrix} \\
&+ \begin{bmatrix} \left(\int_{H_\mathbf{x}} \left(\mu(\mathbf{x}') - \mu(\mathbf{x})\right) \mathrm{g}^{01}(\boldsymbol{\xi}) \mathrm{d}V'\right)\left(\int_{H_\mathbf{x}} \left(\left(v_1(\mathbf{x}') - v_1(\mathbf{x})\right) \mathrm{g}^{01}(\boldsymbol{\xi}) + \left(v_2(\mathbf{x}') - v_2(\mathbf{x})\right) \mathrm{g}^{10}(\boldsymbol{\xi})\right) \mathrm{d}V'\right) \\ \left(\int_{H_\mathbf{x}} \left(\mu(\mathbf{x}') - \mu(\mathbf{x})\right) \mathrm{g}^{10}(\boldsymbol{\xi}) \mathrm{d}V'\right)\left(\int_{H_\mathbf{x}} \left(\left(v_1(\mathbf{x}') - v_1(\mathbf{x})\right) \mathrm{g}^{01}(\boldsymbol{\xi}) + \left(v_2(\mathbf{x}') - v_2(\mathbf{x})\right) \mathrm{g}^{10}(\boldsymbol{\xi})\right) \mathrm{d}V'\right) \end{bmatrix}
\end{aligned} \quad (28)$$

The non-local form of the term $\mathbf{v} \cdot \nabla \mathbf{v}$ can be calculated by using Eq. (17a-b) as

$$\mathbf{v} \cdot \nabla \mathbf{v} = \begin{bmatrix} v_1 \dfrac{\partial v_1}{\partial x_1} + v_2 \dfrac{\partial v_1}{\partial x_2} \\ v_1 \dfrac{\partial v_2}{\partial x_1} + v_2 \dfrac{\partial v_2}{\partial x_2} \end{bmatrix} = \begin{bmatrix} \int_{H_\mathbf{x}} \left(v_1(\mathbf{x}') - v_1(\mathbf{x})\right)\left(v_1(\mathbf{x}) \mathrm{g}^{10}(\boldsymbol{\xi}) + v_2(\mathbf{x}) \mathrm{g}^{01}(\boldsymbol{\xi})\right) \mathrm{d}V' \\ \int_{H_\mathbf{x}} \left(v_2(\mathbf{x}') - v_2(\mathbf{x})\right)\left(v_1(\mathbf{x}) \mathrm{g}^{10}(\boldsymbol{\xi}) + v_2(\mathbf{x}) \mathrm{g}^{01}(\boldsymbol{\xi})\right) \mathrm{d}V' \end{bmatrix} \quad (29)$$

Therefore, the non-local form of the equation for the conservation of momentum becomes

$$
\begin{aligned}
&\rho(\mathbf{x})\begin{Bmatrix}\dfrac{\partial v_1(\mathbf{x})}{\partial t}\\ \dfrac{\partial v_2(\mathbf{x})}{\partial t}\end{Bmatrix}=\\
&-\begin{bmatrix}\int_{H_\mathbf{x}}\left(p(\mathbf{x}')-p(\mathbf{x})\right)\mathrm{g}^{10}(\xi)\mathrm{d}V'\\ \int_{H_\mathbf{x}}\left(p(\mathbf{x}')-p(\mathbf{x})\right)\mathrm{g}^{01}(\xi)\mathrm{d}V'\end{bmatrix}+\mu\begin{bmatrix}\int_{H_\mathbf{x}}\left(v_1(\mathbf{x}')-v_1(\mathbf{x})\right)\left(\mathrm{g}^{20}(\xi)+\mathrm{g}^{02}(\xi)\right)\mathrm{d}V'\\ \int_{H_\mathbf{x}}\left(v_2(\mathbf{x}')-v_2(\mathbf{x})\right)\left(\mathrm{g}^{20}(\xi)+\mathrm{g}^{02}(\xi)\right)\mathrm{d}V'\end{bmatrix}\\
&+\begin{bmatrix}2\left(\int_{H_\mathbf{x}}\left(\mu(\mathbf{x}')-\mu(\mathbf{x})\right)\mathrm{g}^{10}(\xi)\mathrm{d}V'\right)\left(\int_{H_\mathbf{x}}\left(v_1(\mathbf{x}')-v_1(\mathbf{x})\right)\mathrm{g}^{10}(\xi)\mathrm{d}V'\right)\\ 2\left(\int_{H_\mathbf{x}}\left(\mu(\mathbf{x}')-\mu(\mathbf{x})\right)\mathrm{g}^{01}(\xi)\mathrm{d}V'\right)\left(\int_{H_\mathbf{x}}\left(v_2(\mathbf{x}')-v_2(\mathbf{x})\right)\mathrm{g}^{01}(\xi)\mathrm{d}V'\right)\end{bmatrix}\\
&+\begin{bmatrix}\left(\int_{H_\mathbf{x}}\left(\mu(\mathbf{x}')-\mu(\mathbf{x})\right)\mathrm{g}^{01}(\xi)\mathrm{d}V'\right)\left(\int_{H_\mathbf{x}}\begin{pmatrix}\left(v_1(\mathbf{x}')-v_1(\mathbf{x})\right)\mathrm{g}^{01}(\xi)\\ +\left(v_2(\mathbf{x}')-v_2(\mathbf{x})\right)\mathrm{g}^{10}(\xi)\end{pmatrix}\mathrm{d}V'\right)\\ \left(\int_{H_\mathbf{x}}\left(\mu(\mathbf{x}')-\mu(\mathbf{x})\right)\mathrm{g}^{10}(\xi)\mathrm{d}V'\right)\left(\int_{H_\mathbf{x}}\begin{pmatrix}\left(v_1(\mathbf{x}')-v_1(\mathbf{x})\right)\mathrm{g}^{01}(\xi)\\ +\left(v_2(\mathbf{x}')-v_2(\mathbf{x})\right)\mathrm{g}^{10}(\xi)\end{pmatrix}\mathrm{d}V'\right)\end{bmatrix}\\
&-\rho(\mathbf{x})\begin{bmatrix}\int_{H_\mathbf{x}}\left(v_1(\mathbf{x}')-v_1(\mathbf{x})\right)\left(v_1(\mathbf{x})\mathrm{g}^{10}(\xi)+v_2(\mathbf{x})\mathrm{g}^{01}(\xi)\right)\mathrm{d}V'\\ \int_{H_\mathbf{x}}\left(v_2(\mathbf{x}')-v_2(\mathbf{x})\right)\left(v_1(\mathbf{x})\mathrm{g}^{10}(\xi)+v_2(\mathbf{x})\mathrm{g}^{01}(\xi)\right)\mathrm{d}V'\end{bmatrix}+\rho(\mathbf{x})\mathbf{g}
\end{aligned}
\tag{30}
$$

If the viscosity $\mu(\mathbf{x})$ is assumed as uniform and constant, Eq.(30) reduces to

$$
\begin{aligned}
&\rho(\mathbf{x})\begin{Bmatrix}\dfrac{\partial v_1(\mathbf{x})}{\partial t}\\ \dfrac{\partial v_2(\mathbf{x})}{\partial t}\end{Bmatrix}=\\
&-\begin{bmatrix}\int_{H_\mathbf{x}}\left(p(\mathbf{x}')-p(\mathbf{x})\right)\mathrm{g}^{10}(\xi)\mathrm{d}V'\\ \int_{H_\mathbf{x}}\left(p(\mathbf{x}')-p(\mathbf{x})\right)\mathrm{g}^{01}(\xi)\mathrm{d}V'\end{bmatrix}+\mu\begin{bmatrix}\int_{H_\mathbf{x}}\left(v_1(\mathbf{x}')-v_1(\mathbf{x})\right)\left(\mathrm{g}^{20}(\xi)+\mathrm{g}^{02}(\xi)\right)\mathrm{d}V'\\ \int_{H_\mathbf{x}}\left(v_2(\mathbf{x}')-v_2(\mathbf{x})\right)\left(\mathrm{g}^{20}(\xi)+\mathrm{g}^{02}(\xi)\right)\mathrm{d}V'\end{bmatrix}\\
&-\rho(\mathbf{x})\begin{bmatrix}\int_{H_\mathbf{x}}\left(v_1(\mathbf{x}')-v_1(\mathbf{x})\right)\left(v_1(\mathbf{x})\mathrm{g}^{10}(\xi)+v_2(\mathbf{x})\mathrm{g}^{01}(\xi)\right)\mathrm{d}V'\\ \int_{H_\mathbf{x}}\left(v_2(\mathbf{x}')-v_2(\mathbf{x})\right)\left(v_1(\mathbf{x})\mathrm{g}^{10}(\xi)+v_2(\mathbf{x})\mathrm{g}^{01}(\xi)\right)\mathrm{d}V'\end{bmatrix}+\rho(\mathbf{x})\mathbf{g}
\end{aligned}
\tag{31}
$$

3.4 Conservation of Energy

For incompressible fluid flows, the local form of the conservation of energy is [41]

$$
\rho\left(\frac{\partial e}{\partial t}+\mathbf{v}\cdot\nabla e\right)=-\nabla\cdot\mathbf{q}+\boldsymbol{\sigma}:\nabla\otimes\mathbf{v}+Q \tag{32}
$$

where e is the internal energy, Q is the internal heat generation, and $\mathbf{q}$ is the heat flux vector defined as

$$\mathbf{q} = -k(\mathbf{x}) \cdot \nabla T \tag{33}$$

where $k(\mathbf{x})$ is the thermal conductivity.

For thermodynamic systems, the internal energy assumed to be a function of temperature and density, i.e. $e = e(T, \rho)$. For constant density, the specific heat capacity under constant pressure, c_p, is equal to the specific heat capacity under constant volume, c_v, i.e. $c_v = c_p = C$ [41]. Consequently, the time rate of change of the internal energy can be evaluated as [41]

$$\frac{\partial e}{\partial t} + \mathbf{v} \cdot \nabla e = C\left(\frac{\partial T}{\partial t} + \mathbf{v} \cdot \nabla T\right) = C\left(\frac{\partial T}{\partial t} + v_1 \frac{\partial T}{\partial x_1} + v_2 \frac{\partial T}{\partial x_2}\right) \tag{34}$$

where C represents the specific heat capacity. By using the definition of stress in Eq.(20), the term $\boldsymbol{\sigma} : \nabla \otimes \mathbf{v}$ can be written as [41]

$$\boldsymbol{\sigma} : \nabla \otimes \mathbf{v} = -p\mathbf{I} : (\nabla \otimes \mathbf{v}) + \mu(\nabla \otimes \mathbf{v}) : (\nabla \otimes \mathbf{v}) + \mu(\nabla \otimes \mathbf{v})^T : (\nabla \otimes \mathbf{v}) \tag{35}$$

or

$$\boldsymbol{\sigma} : \nabla \otimes \mathbf{v} = -p\left(\frac{\partial v_1}{\partial x_1} + \frac{\partial v_2}{\partial x_2}\right) + \mu\left(2\left(\frac{\partial v_1}{\partial x_1}\right)^2 + 2\left(\frac{\partial v_2}{\partial x_2}\right)^2 + \left(\frac{\partial v_1}{\partial x_2} + \frac{\partial v_2}{\partial x_1}\right)^2\right) \tag{36}$$

Substituting the incompressible condition Eq. (19) into Eq. (36) results in [41]

$$\boldsymbol{\sigma} : \nabla \otimes \mathbf{v} = \mu\left(2\left(\frac{\partial v_1}{\partial x_1}\right)^2 + 2\left(\frac{\partial v_2}{\partial x_2}\right)^2 + \left(\frac{\partial v_1}{\partial x_2} + \frac{\partial v_2}{\partial x_1}\right)^2\right) \tag{37}$$

By substituting Eq.(33), Eq.(34) and Eq.(37) into Eq.(32), the conservation of energy equation becomes [41]

$$\rho C\frac{\partial T}{\partial t}=\frac{\partial k}{\partial x_1}\frac{\partial T}{\partial x_1}+\frac{\partial k}{\partial x_2}\frac{\partial T}{\partial x_2}+k\left(\frac{\partial^2 T}{\partial x_1^2}+\frac{\partial^2 T}{\partial x_2^2}\right)$$
$$+\mu\left(2\left(\frac{\partial v_1}{\partial x_1}\right)^2+2\left(\frac{\partial v_2}{\partial x_2}\right)^2+\left(\frac{\partial v_1}{\partial x_2}+\frac{\partial v_2}{\partial x_1}\right)^2\right)-\rho C\left(v_1\frac{\partial T}{\partial x_1}+v_2\frac{\partial T}{\partial x_2}\right)+Q \tag{38}$$

By using Eq.(9), the non-local form of the differentials in Eq.(38) can be expressed as

$$\frac{\partial k(\mathbf{x})}{\partial x_1}=\int_{H_\mathbf{x}}\left(k(\mathbf{x}')-k(\mathbf{x})\right)\mathrm{g}^{10}(\boldsymbol{\xi})\mathrm{d}V';\ \frac{\partial k(\mathbf{x})}{\partial x_2}=\int_{H_\mathbf{x}}\left(k(\mathbf{x}')-k(\mathbf{x})\right)\mathrm{g}^{01}(\boldsymbol{\xi})\mathrm{d}V' \tag{39a}$$

$$\frac{\partial T(\mathbf{x})}{\partial x_1}=\int_{H_\mathbf{x}}\left(T(\mathbf{x}')-T(\mathbf{x})\right)\mathrm{g}^{10}(\boldsymbol{\xi})\mathrm{d}V';\ \frac{\partial T(\mathbf{x})}{\partial x_2}=\int_{H_\mathbf{x}}\left(T(\mathbf{x}')-T(\mathbf{x})\right)\mathrm{g}^{01}(\boldsymbol{\xi})\mathrm{d}V'; \tag{39b}$$

$$\frac{\partial^2 T(\mathbf{x})}{\partial x_1^2}=\int_{H_\mathbf{x}}\left(T(\mathbf{x}')-T(\mathbf{x})\right)\mathrm{g}^{20}(\boldsymbol{\xi})\mathrm{d}V';\ \frac{\partial^2 T(\mathbf{x})}{\partial x_2^2}=\int_{H_\mathbf{x}}\left(T(\mathbf{x}')-T(\mathbf{x})\right)\mathrm{g}^{02}(\boldsymbol{\xi})\mathrm{d}V' \tag{39c}$$

Therefore, by substituting the non-local form of the differentials provided in Eq. (17) and Eq. (39) into Eq.(38), the non-local form of conservation of energy becomes

$$\begin{aligned}
&\rho(\mathbf{x})C\frac{\partial T(\mathbf{x})}{\partial t}=\\
&\left(\int_{H_\mathbf{x}}\left(k(\mathbf{x}')-k(\mathbf{x})\right)g^{10}(\boldsymbol{\xi})\mathrm{d}V'\right)\left(\int_{H_\mathbf{x}}\left(T(\mathbf{x}')-T(\mathbf{x})\right)g^{10}(\boldsymbol{\xi})\mathrm{d}V'\right)\\
&+\left(\int_{H_\mathbf{x}}\left(k(\mathbf{x}')-k(\mathbf{x})\right)g^{01}(\boldsymbol{\xi})\mathrm{d}V'\right)\left(\int_{H_\mathbf{x}}\left(T(\mathbf{x}')-T(\mathbf{x})\right)g^{01}(\boldsymbol{\xi})\mathrm{d}V'\right)\\
&+k(\mathbf{x})\int_{H_\mathbf{x}}\left(T(\mathbf{x}')-T(\mathbf{x})\right)\left(g^{20}(\boldsymbol{\xi})+g^{02}(\boldsymbol{\xi})\right)\mathrm{d}V'\\
&+\mu(\mathbf{x})\left(\begin{array}{l}2\left(\int_{H_\mathbf{x}}\left(v_1(\mathbf{x}')-v_1(\mathbf{x})\right)g^{10}(\boldsymbol{\xi})\mathrm{d}V'\right)^2+2\left(\int_{H_\mathbf{x}}\left(v_2(\mathbf{x}')-v_2(\mathbf{x})\right)g^{01}(\boldsymbol{\xi})\mathrm{d}V'\right)^2\\+\left(\int_{H_\mathbf{x}}\left(\left(v_1(\mathbf{x}')-v_1(\mathbf{x})\right)g^{01}(\boldsymbol{\xi})+\left(v_2(\mathbf{x}')-v_2(\mathbf{x})\right)g^{10}(\boldsymbol{\xi})\right)\mathrm{d}V'\right)^2\end{array}\right)\\
&-\rho(\mathbf{x})C\int_{H_\mathbf{x}}\left(T(\mathbf{x}')-T(\mathbf{x})\right)\left(v_1(\mathbf{x})g^{10}(\boldsymbol{\xi})+v_2(\mathbf{x})g^{01}(\boldsymbol{\xi})\right)\mathrm{d}V'+Q
\end{aligned} \tag{40}$$

If the thermal conductivity $k(\mathbf{x})$ is assumed to be uniform and constant, Eq.(40) reduces to

$$
\begin{aligned}
&\rho(\mathbf{x})C\frac{\partial T(\mathbf{x})}{\partial t}=k(\mathbf{x})\int_{H_{\mathbf{x}}}\left(T(\mathbf{x}')-T(\mathbf{x})\right)\left(g^{20}(\boldsymbol{\xi})+g^{02}(\boldsymbol{\xi})\right)\mathrm{d}V' \\
&+\mu(\mathbf{x})\begin{pmatrix} 2\left(\int_{H_{\mathbf{x}}}\left(v_1(\mathbf{x}')-v_1(\mathbf{x})\right)g^{10}(\boldsymbol{\xi})\mathrm{d}V'\right)^2+2\left(\int_{H_{\mathbf{x}}}\left(v_2(\mathbf{x}')-v_2(\mathbf{x})\right)g^{01}(\boldsymbol{\xi})\mathrm{d}V'\right)^2 \\ +\left(\int_{H_{\mathbf{x}}}\left(\left(v_1(\mathbf{x}')-v_1(\mathbf{x})\right)g^{01}(\boldsymbol{\xi})+\left(v_2(\mathbf{x}')-v_2(\mathbf{x})\right)g^{10}(\boldsymbol{\xi})\right)\mathrm{d}V'\right)^2 \end{pmatrix} \\
&-\rho(\mathbf{x})C\int_{H_{\mathbf{x}}}\left(T(\mathbf{x}')-T(\mathbf{x})\right)\left(v_1(\mathbf{x})g^{10}(\boldsymbol{\xi})+v_2(\mathbf{x})g^{01}(\boldsymbol{\xi})\right)\mathrm{d}V' \\
&+Q
\end{aligned}
\tag{41}
$$

3.5 Non-dimensional Form of Governing Equations

The governing equations in a non-dimensional form can be obtained by using following non-dimensional parameters [6]

$$
x_i^*=\frac{x_i}{L_0},\ v_i^*=\frac{v_i}{v_0},\ t^*=\frac{tv_0}{L_0},\ \rho^*=\frac{\rho}{\rho_0},\ \mu^*=\frac{\mu}{\mu_0},\ k^*=\frac{k}{k_0},\ T^*=\frac{T}{T_0},\ p^*=\frac{p}{\rho_0 v_0^2},\ g^*=\frac{gL_0}{v_0^2} \tag{42}
$$

where the subscript $\left(_0\right)$ represents the reference variable and the superscript $\left(^*\right)$ represents the non-dimensional variable.

The non-dimensional form of the local governing equations by ignoring the internal heat generation can be written as

Conservation of mass

$$
\frac{\partial\rho^*}{\partial t^*}+\left(v_1^*\frac{\partial\rho^*}{\partial x_1^*}+v_2^*\frac{\partial\rho^*}{\partial x_2^*}\right)=-\rho^*\left(\frac{\partial v_1^*}{\partial x_1^*}+\frac{\partial v_2^*}{\partial x_2^*}\right) \tag{43a}
$$

Conservation of momentum

$$
\begin{aligned}
&\begin{bmatrix} \dfrac{\partial v_1^*}{\partial t^*}+v_1^*\dfrac{\partial v_1^*}{\partial x_1^*}+v_2^*\dfrac{\partial v_1^*}{\partial x_2^*} \\ \dfrac{\partial v_2^*}{\partial t^*}+v_1^*\dfrac{\partial v_2^*}{\partial x_1^*}+v_2^*\dfrac{\partial v_2^*}{\partial x_2^*} \end{bmatrix}= \\
&-\begin{bmatrix} \dfrac{\partial p^*}{\partial x_1^*} \\ \dfrac{\partial p^*}{\partial x_2^*} \end{bmatrix}+\frac{1}{\mathrm{Re}}\begin{bmatrix} \mu^*\left(\dfrac{\partial^2 v_1^*}{\partial x_1^{*2}}+\dfrac{\partial^2 v_1^*}{\partial x_2^{*2}}\right)+2\dfrac{\partial\mu^*}{\partial x_1^*}\dfrac{\partial v_1^*}{\partial x_1^*}+\dfrac{\partial\mu^*}{\partial x_2^*}\left(\dfrac{\partial v_1^*}{\partial x_2^*}+\dfrac{\partial v_2^*}{\partial x_1^*}\right) \\ \mu^*\left(\dfrac{\partial^2 v_2^*}{\partial x_1^{*2}}+\dfrac{\partial^2 v_2^*}{\partial x_2^{*2}}\right)+2\dfrac{\partial\mu^*}{\partial x_2^*}\dfrac{\partial v_2^*}{\partial x_2^*}+\dfrac{\partial\mu^*}{\partial x_1^*}\left(\dfrac{\partial v_1^*}{\partial x_2^*}+\dfrac{\partial v_2^*}{\partial x_1^*}\right) \end{bmatrix}+\begin{bmatrix} 0 \\ g^* \end{bmatrix}
\end{aligned}
\tag{43b}
$$

Conservation of energy

$$\rho^*\left(\frac{\partial T^*}{\partial t^*}+v_1^*\frac{\partial T^*}{\partial x_1^*}+v_2\frac{\partial T^*}{\partial x_2^*}\right)=\frac{1}{\mathrm{Re}\,\mathrm{Pr}}\left(\frac{\partial k^*}{\partial x_1^*}\frac{\partial T^*}{\partial x_1^*}+\frac{\partial k^*}{\partial x_2^*}\frac{\partial T^*}{\partial x_2^*}\right)+\frac{k^*}{\mathrm{Re}\,\mathrm{Pr}}\left(\frac{\partial^2 T^*}{\partial x_1^{*2}}+\frac{\partial^2 T^*}{\partial x_2^{*2}}\right)$$
$$+\frac{\mathrm{Ec}}{\mathrm{Re}}\mu^*\left(2\left(\frac{\partial v_1^*}{\partial x_1^*}\right)^2+2\left(\frac{\partial v_2^*}{\partial x_2^*}\right)^2+\left(\frac{\partial v_1^*}{\partial x_2^*}+\frac{\partial v_2^*}{\partial x_1^*}\right)^2\right) \tag{43c}$$

The non-dimensional parameters in Eq. (43) are defined as

$$\mathrm{Re}=\frac{\rho_0 v_0 L_0}{\mu_0},\ \mathrm{Pr}=\frac{\mu_0 C_0}{k_0},\ \mathrm{Ec}=\frac{v_0^2}{C_0 T_0} \tag{44}$$

where Re is the Reynolds number, Pr is the Prandtl number, and Ec is the Eckert number.

Similarly, the non-local governing equations in Eq.(18), Eq.(30), and Eq.(40) can also be written into their non-dimensional forms as

Conservation of mass

$$\frac{\partial \rho^*\left(\mathbf{x}^*\right)}{\partial t^*}=-\rho^*\left(\mathbf{x}^*\right)\int_{H_{\mathbf{x}^*}}\left(\left(v_1^*\left(\mathbf{x}'^*\right)-v_1^*\left(\mathbf{x}^*\right)\right)\mathrm{g}^{10}\left(\boldsymbol{\xi}^*\right)+\left(v_2^*\left(\mathbf{x}'^*\right)-v_2^*\left(\mathbf{x}^*\right)\right)\mathrm{g}^{01}\left(\boldsymbol{\xi}^*\right)\right)\mathrm{d}V'^*$$
$$-\int_{H_{\mathbf{x}^*}}\left(\rho^*\left(\mathbf{x}'^*\right)-\rho\left(\mathbf{x}^*\right)\right)\left(v_1\left(\mathbf{x}^*\right)\mathrm{g}^{10}\left(\boldsymbol{\xi}^*\right)+v_2\left(\mathbf{x}^*\right)\mathrm{g}^{01}\left(\boldsymbol{\xi}^*\right)\right)\mathrm{d}V'^* \tag{45a}$$

Conservation of momentum

$$
\begin{aligned}
&\begin{bmatrix} \dfrac{\partial v_1^*(\mathbf{x}^*)}{\partial t^*} \\ \dfrac{\partial v_2^*(\mathbf{x}^*)}{\partial t^*} \end{bmatrix} = -\begin{bmatrix} \int_{H_{\mathbf{x}^*}} \left(p^*(\mathbf{x}'^*) - p^*(\mathbf{x}^*)\right) g^{10}(\boldsymbol{\xi}^*)\,\mathrm{d}V'^* \\ \int_{H_{\mathbf{x}^*}} \left(p^*(\mathbf{x}'^*) - p^*(\mathbf{x}^*)\right) g^{01}(\boldsymbol{\xi}^*)\,\mathrm{d}V'^* \end{bmatrix} \\
&+\frac{\mu^*(\mathbf{x}^*)}{\mathrm{Re}} \begin{bmatrix} \int_{H_{\mathbf{x}^*}} \left(v_1^*(\mathbf{x}'^*) - v_1^*(\mathbf{x}^*)\right)\left(\mathrm{g}^{20}(\boldsymbol{\xi}^*) + \mathrm{g}^{02}(\boldsymbol{\xi}^*)\right)\mathrm{d}V'^* \\ \int_{H_{\mathbf{x}^*}} \left(v_2^*(\mathbf{x}'^*) - v_2^*(\mathbf{x}^*)\right)\left(\mathrm{g}^{20}(\boldsymbol{\xi}^*) + \mathrm{g}^{02}(\boldsymbol{\xi}^*)\right)\mathrm{d}V'^* \end{bmatrix} \\
&+\frac{2}{\mathrm{Re}} \begin{bmatrix} \left(\int_{H_{\mathbf{x}^*}} \left(\mu^*(\mathbf{x}'^*) - \mu^*(\mathbf{x}^*)\right)\mathrm{g}^{10}(\boldsymbol{\xi}^*)\,\mathrm{d}V'^*\right)\left(\int_{H_{\mathbf{x}^*}} \left(v_1^*(\mathbf{x}'^*) - v_1^*(\mathbf{x}^*)\right)\mathrm{g}^{10}(\boldsymbol{\xi}^*)\,\mathrm{d}V'^*\right) \\ \left(\int_{H_{\mathbf{x}^*}} \left(\mu^*(\mathbf{x}'^*) - \mu^*(\mathbf{x}^*)\right)\mathrm{g}^{01}(\boldsymbol{\xi}^*)\,\mathrm{d}V'^*\right)\left(\int_{H_{\mathbf{x}^*}} \left(v_2^*(\mathbf{x}'^*) - v_2^*(\mathbf{x}^*)\right)\mathrm{g}^{01}(\boldsymbol{\xi}^*)\,\mathrm{d}V'^*\right) \end{bmatrix} \\
&+\frac{1}{\mathrm{Re}} \begin{bmatrix} \left(\int_{H_{\mathbf{x}^*}} \left(\mu^*(\mathbf{x}'^*) - \mu^*(\mathbf{x}^*)\right)\mathrm{g}^{01}(\boldsymbol{\xi}^*)\,\mathrm{d}V'^*\right)\left(\int_{H_{\mathbf{x}^*}} \begin{pmatrix} \left(v_1^*(\mathbf{x}'^*) - v_1^*(\mathbf{x}^*)\right)\mathrm{g}^{01}(\boldsymbol{\xi}^*) \\ +\left(v_2^*(\mathbf{x}'^*) - v_2^*(\mathbf{x}^*)\right)\mathrm{g}^{10}(\boldsymbol{\xi}^*) \end{pmatrix}\mathrm{d}V'^*\right) \\ \left(\int_{H_{\mathbf{x}^*}} \left(\mu^*(\mathbf{x}'^*) - \mu^*(\mathbf{x}^*)\right)\mathrm{g}^{10}(\boldsymbol{\xi}^*)\,\mathrm{d}V'^*\right)\left(\int_{H_{\mathbf{x}^*}} \begin{pmatrix} \left(v_1^*(\mathbf{x}'^*) - v_1^*(\mathbf{x}^*)\right)\mathrm{g}^{01}(\boldsymbol{\xi}^*) \\ +\left(v_2^*(\mathbf{x}'^*) - v_2^*(\mathbf{x}^*)\right)\mathrm{g}^{10}(\boldsymbol{\xi}^*) \end{pmatrix}\mathrm{d}V'^*\right) \end{bmatrix} \\
&-\begin{bmatrix} \int_{H_{\mathbf{x}^*}} \left(v_1^*(\mathbf{x}'^*) - v_1^*(\mathbf{x}^*)\right)\left(v_1^*(\mathbf{x}^*)\mathrm{g}^{10}(\boldsymbol{\xi}^*) + v_2^*(\mathbf{x}^*)\mathrm{g}^{01}(\boldsymbol{\xi}^*)\right)\mathrm{d}V'^* \\ \int_{H_{\mathbf{x}^*}} \left(v_2^*(\mathbf{x}'^*) - v_2^*(\mathbf{x}^*)\right)\left(v_1^*(\mathbf{x}^*)\mathrm{g}^{10}(\boldsymbol{\xi}^*) + v_2^*(\mathbf{x}^*)\mathrm{g}^{01}(\boldsymbol{\xi}^*)\right)\mathrm{d}V'^* \end{bmatrix} + \begin{bmatrix} 0 \\ g^* \end{bmatrix}
\end{aligned}
\tag{45b}
$$

Conservation of energy

$$
\begin{aligned}
&\rho^*(\mathbf{x}^*)\frac{\partial T^*(\mathbf{x}^*)}{\partial t^*} = \\
&+\frac{1}{\mathrm{Re}\,\mathrm{Pr}} \begin{pmatrix} \left(\int_{H_{\mathbf{x}^*}} \left(k^*(\mathbf{x}'^*) - k^*(\mathbf{x}^*)\right)\mathrm{g}^{01}(\boldsymbol{\xi}^*)\,\mathrm{d}V'^*\right)\left(\int_{H_{\mathbf{x}^*}} \left(T^*(\mathbf{x}'^*) - T^*(\mathbf{x}^*)\right)\mathrm{g}^{01}(\boldsymbol{\xi}^*)\,\mathrm{d}V'^*\right) \\ +\left(\int_{H_{\mathbf{x}^*}} \left(k^*(\mathbf{x}'^*) - k^*(\mathbf{x}^*)\right)\mathrm{g}^{10}(\boldsymbol{\xi}^*)\,\mathrm{d}V'^*\right)\left(\int_{H_{\mathbf{x}^*}} \left(T^*(\mathbf{x}'^*) - T^*(\mathbf{x}^*)\right)\mathrm{g}^{10}(\boldsymbol{\xi}^*)\,\mathrm{d}V'^*\right) \end{pmatrix} \\
&+\frac{k^*(\mathbf{x}^*)}{\mathrm{Re}\,\mathrm{Pr}} \int_{H_{\mathbf{x}^*}} \left(T^*(\mathbf{x}'^*) - T^*(\mathbf{x}^*)\right)\left(g^{20}(\boldsymbol{\xi}^*) + g^{02}(\boldsymbol{\xi}^*)\right)\mathrm{d}V'^* \\
&+\frac{\mathrm{Ec}\,\mu^*(\mathbf{x}^*)}{\mathrm{Re}} \begin{pmatrix} 2\left(\int_{H_{\mathbf{x}^*}} \left(v_1^*(\mathbf{x}'^*) - v_1^*(\mathbf{x}^*)\right)g^{10}(\boldsymbol{\xi}^*)\,\mathrm{d}V'^*\right)^2 \\ +2\left(\int_{H_{\mathbf{x}^*}} \left(v_2^*(\mathbf{x}'^*) - v_2^*(\mathbf{x}^*)\right)g^{01}(\boldsymbol{\xi}^*)\,\mathrm{d}V'^*\right)^2 \\ +\left(\int_{H_{\mathbf{x}^*}} \left(\left(v_1^*(\mathbf{x}'^*) - v_1^*(\mathbf{x}^*)\right)g^{01}(\boldsymbol{\xi}^*) + \left(v_2^*(\mathbf{x}'^*) - v_2^*(\mathbf{x}^*)\right)g^{10}(\boldsymbol{\xi}^*)\right)\mathrm{d}V'^*\right)^2 \end{pmatrix} \\
&-\rho^*(\mathbf{x}^*)\int_{H_{\mathbf{x}^*}} \left(T^*(\mathbf{x}'^*) - T^*(\mathbf{x}^*)\right)\left(v_1^*(\mathbf{x}^*)g^{10}(\boldsymbol{\xi}^*) + v_2^*(\mathbf{x}^*)g^{01}(\boldsymbol{\xi}^*)\right)\mathrm{d}V'^*
\end{aligned}
\tag{45c}
$$

where the non-dimensional relative position is calculated as $\boldsymbol{\xi}^* = \mathbf{x}'^* - \mathbf{x}^*$.

Furthermore, if the viscosity and the thermal conductivity are assumed to be uniform and constant, Eq. (45b) and Eq. (45c) reduce to

$$\begin{aligned}
&\begin{bmatrix} \dfrac{\partial v_1^*(\mathbf{x}^*)}{\partial t^*} \\ \dfrac{\partial v_2^*(\mathbf{x}^*)}{\partial t^*} \end{bmatrix} = -\begin{bmatrix} \int_{H_{\mathbf{x}^*}} \left(p^*(\mathbf{x}'^*) - p^*(\mathbf{x}^*)\right) g^{10}(\xi^*)\,\mathrm{d}V'^* \\ \int_{H_{\mathbf{x}^*}} \left(p^*(\mathbf{x}'^*) - p^*(\mathbf{x}^*)\right) g^{01}(\xi^*)\,\mathrm{d}V'^* \end{bmatrix} \\
&+\frac{\mu^*(\mathbf{x}^*)}{\mathrm{Re}}\begin{bmatrix} \int_{H_{\mathbf{x}^*}} \left(v_1^*(\mathbf{x}'^*) - v_1^*(\mathbf{x}^*)\right)\left(\mathrm{g}^{20}(\xi^*) + \mathrm{g}^{02}(\xi^*)\right)\mathrm{d}V'^* \\ \int_{H_{\mathbf{x}^*}} \left(v_2^*(\mathbf{x}'^*) - v_2^*(\mathbf{x}^*)\right)\left(\mathrm{g}^{20}(\xi^*) + \mathrm{g}^{02}(\xi^*)\right)\mathrm{d}V'^* \end{bmatrix} \\
&-\begin{bmatrix} \int_{H_{\mathbf{x}^*}} \left(v_1^*(\mathbf{x}'^*) - v_1^*(\mathbf{x}^*)\right)\left(v_1^*(\mathbf{x}^*)\mathrm{g}^{10}(\xi^*) + v_2^*(\mathbf{x}^*)\mathrm{g}^{01}(\xi^*)\right)\mathrm{d}V'^* \\ \int_{H_{\mathbf{x}^*}} \left(v_2^*(\mathbf{x}'^*) - v_2^*(\mathbf{x}^*)\right)\left(v_1^*(\mathbf{x}^*)\mathrm{g}^{10}(\xi^*) + v_2^*(\mathbf{x}^*)\mathrm{g}^{01}(\xi^*)\right)\mathrm{d}V'^* \end{bmatrix} + \begin{bmatrix} 0 \\ g^* \end{bmatrix}
\end{aligned} \tag{46}$$

$$\begin{aligned}
&\rho^*(\mathbf{x}^*)\frac{\partial T^*(\mathbf{x}^*)}{\partial t^*} = \frac{k^*(\mathbf{x}^*)}{\mathrm{Re}\,\mathrm{Pr}}\int_{H_{\mathbf{x}^*}} \left(T^*(\mathbf{x}'^*) - T^*(\mathbf{x}^*)\right)\left(g^{20}(\xi^*) + g^{02}(\xi^*)\right)\mathrm{d}V'^* \\
&+\frac{\mathrm{Ec}\mu^*(\mathbf{x}^*)}{\mathrm{Re}}\begin{pmatrix} 2\left(\int_{H_{\mathbf{x}^*}} \left(v_1^*(\mathbf{x}'^*) - v_1^*(\mathbf{x}^*)\right) g^{10}(\xi^*)\,\mathrm{d}V'^*\right)^2 \\ +2\left(\int_{H_{\mathbf{x}^*}} \left(v_2^*(\mathbf{x}'^*) - v_2^*(\mathbf{x}^*)\right) g^{01}(\xi^*)\,\mathrm{d}V'^*\right)^2 \\ +\left(\int_{H_{\mathbf{x}^*}} \left(\left(v_1^*(\mathbf{x}'^*) - v_1^*(\mathbf{x}^*)\right) g^{01}(\xi^*) + \left(v_2^*(\mathbf{x}'^*) - v_2^*(\mathbf{x}^*)\right) g^{10}(\xi^*)\right)\mathrm{d}V'^*\right)^2 \end{pmatrix} \\
&-\rho^*(\mathbf{x}^*)\int_{H_{\mathbf{x}^*}} \left(T^*(\mathbf{x}'^*) - T^*(\mathbf{x}^*)\right)\left(v_1^*(\mathbf{x}^*) g^{10}(\xi^*) + v_2^*(\mathbf{x}^*) g^{01}(\xi^*)\right)\mathrm{d}V'^*
\end{aligned} \tag{47}$$

The local Nusselt numbers are defined as

$$\mathrm{Nu}_{\mathrm{loc}}(x) = \left|\frac{\partial T^*}{\partial y^*}\right|_{y=\mathrm{loc}} \tag{48a}$$

$$\mathrm{Nu}_{\mathrm{loc}}(y) = \left|\frac{\partial T^*}{\partial x^*}\right|_{x=\mathrm{loc}} \tag{48b}$$

By substituting Eq. (39b) into Eq. (48), the Nusselt numbers can be calculated in PD approach as

$$\mathrm{Nu}_{\mathrm{loc}}(x) = \left|\int_{H_{\mathbf{x}}} \left(T(\mathbf{x}'^*) - T(\mathbf{x}^*)\right)\mathrm{g}^{01}(\xi^*)\,\mathrm{d}V'^*\right|_{y=\mathrm{loc}} \tag{49a}$$

$$\mathrm{Nu}_{\mathrm{loc}}\left(y\right)=\left|\int_{H_{\mathbf{x}}}\left(T\left(\mathbf{x}'^{*}\right)-T\left(\mathbf{x}^{*}\right)\right)\mathrm{g}^{10}\left(\boldsymbol{\xi}^{*}\right)\mathrm{d}V'^{*}\right|_{x=\mathrm{loc}} \tag{49b}$$

The average Nusselt numbers are defined as

$$\mathrm{Nu}_{x}=\frac{1}{\mathrm{L}}\int_{0}^{L}\mathrm{Nu}_{\mathrm{loc}}\left(x\right)\mathrm{d}x \tag{50a}$$

$$\mathrm{Nu}_{y}=\frac{1}{W}\int_{0}^{L}\mathrm{Nu}_{\mathrm{loc}}(y)\mathrm{d}y \tag{50b}$$

4 NUMERICAL IMPLEMENTATION

4.1 Governing Equations in Discretized Form

The non-local form of the governing equations provided in section 3 can be written in their discrete forms as;

Conservation of mass:

$$\rho_{i}^{n+1}=\rho_{i}^{n}-\Delta t\sum_{j=1}^{N_{i}}\left(\begin{array}{l}\rho_{i}^{n}\left(\begin{array}{l}\left(v_{1,j}^{n}-v_{1,i}^{n}\right)\mathrm{g}^{10}\left(x_{1,j}-x_{1,i},x_{2,j}-x_{2,i}\right)\\+\left(v_{2,j}^{n}-v_{2,i}^{n}\right)\mathrm{g}^{01}\left(x_{1,j}-x_{1,i},x_{2,j}-x_{2,i}\right)\end{array}\right)\\+\left(\rho_{j}^{n}-\rho_{i}^{n}\right)\left(\begin{array}{l}v_{1,i}^{n}\mathrm{g}^{10}\left(x_{1,j}-x_{1,i},x_{2,j}-x_{2,i}\right)\\+v_{2,i}^{n}\mathrm{g}^{01}\left(x_{1,j}-x_{1,i},x_{2,j}-x_{2,i}\right)\end{array}\right)\end{array}\right)V_{j} \tag{51}$$

where i represents the point of interest (shown in red colour in Fig. 2), j represents its family members (shown in green colour in Fig. 2). The parameter N_i represents the total number of the family members of i. The initial coordinates of points i and j are denoted as $\left(x_{1,i},x_{2,i}\right)$ and $\left(x_{1,j},x_{2,j}\right)$. The volume of point j is denoted as V_j. The superscript $\left(^{n}\right)$ represents the current time step. The time step size is Δt.

Conservation of momentum:

$$a_{1,i}^{n}=\frac{1}{\rho_i^{n+1}}\left(\begin{array}{l}
-\sum_{j=1}^{N_i}\left(p_j^n-p_i^n\right)\mathrm{g}^{10}\left(x_{1,j}-x_{1,i},x_{2,j}-x_{2,i}\right)V_j \\
+\mu_i^n\sum_{j=1}^{N_i}\left(v_{1,j}^n-v_{1,i}^n\right)\left(\mathrm{g}^{20}\left(x_{1,j}-x_{1,i},x_{2,j}-x_{2,i}\right)+\mathrm{g}^{02}\left(x_{1,j}-x_{1,i},x_{2,j}-x_{2,i}\right)\right)V_j \\
+2\left(\sum_{j=1}^{N_i}\left(\mu_j^n-\mu_i^n\right)\mathrm{g}^{10}\left(x_{1,j}-x_{1,i},x_{2,j}-x_{2,i}\right)V_j\right)\left(\sum_{j=1}^{N_i}\left(v_{1,j}^n-v_{1,i}^n\right)\mathrm{g}^{10}\left(x_{1,j}-x_{1,i},x_{2,j}-x_{2,i}\right)V_j\right) \\
+\left(\sum_{j=1}^{N_i}\left(\mu_j^n-\mu_i^n\right)\mathrm{g}^{01}\left(x_{1,j}-x_{1,i},x_{2,j}-x_{2,i}\right)V_j\right)\left(\sum_{j=1}^{N_i}\left(\begin{array}{l}\left(v_{1,j}^n-v_{1,i}^n\right)\mathrm{g}^{01}\left(x_{1,j}-x_{1,i},x_{2,j}-x_{2,i}\right) \\ +\left(v_{2,j}^n-v_{2,i}^n\right)\mathrm{g}^{10}\left(x_{1,j}-x_{1,i},x_{2,j}-x_{2,i}\right)\end{array}\right)V_j\right) \\
-\rho_i^{n+1}\sum_{j=1}^{N_i}\left(v_{1,j}^n-v_{1,i}^n\right)\left(v_{1,i}^n\mathrm{g}^{10}\left(x_{1,j}-x_{1,i},x_{2,j}-x_{2,i}\right)+v_{2,i}^n\mathrm{g}^{01}\left(x_{1,j}-x_{1,i},x_{2,j}-x_{2,i}\right)\right)V_j
\end{array}\right) \tag{52a}$$

$$a_{2,i}^{n}=\frac{1}{\rho_i^{n+1}}\left(\begin{array}{l}
-\sum_{j=1}^{N_i}\left(p_j^n-p_i^n\right)\mathrm{g}^{01}\left(x_{1,j}-x_{1,i},x_{2,j}-x_{2,i}\right)V_j+\mu_i^n\sum_{j=1}^{N_i}\left(v_{2,j}^n-v_{2,i}^n\right)\left(\begin{array}{l}\mathrm{g}^{20}\left(x_{1,j}-x_{1,i},x_{2,j}-x_{2,i}\right) \\ +\mathrm{g}^{02}\left(x_{1,j}-x_{1,i},x_{2,j}-x_{2,i}\right)\end{array}\right)V_j \\
+2\left(\sum_{j=1}^{N_i}\left(\mu_j^n-\mu_i^n\right)\mathrm{g}^{01}\left(x_{1,j}-x_{1,i},x_{2,j}-x_{2,i}\right)V_j\right)\left(\sum_{j=1}^{N_i}\left(v_{2,j}^n-v_{2,i}^n\right)\mathrm{g}^{01}\left(x_{1,j}-x_{1,i},x_{2,j}-x_{2,i}\right)V_j\right) \\
+\left(\sum_{j=1}^{N_i}\left(\mu_j^n-\mu_i^n\right)\mathrm{g}^{10}\left(x_{1,j}-x_{1,i},x_{2,j}-x_{2,i}\right)V_j\right)\left(\sum_{j=1}^{N_i}\left(\begin{array}{l}\left(v_{1,j}^n-v_{1,i}^n\right)\mathrm{g}^{01}\left(x_{1,j}-x_{1,i},x_{2,j}-x_{2,i}\right) \\ +\left(v_{2,j}^n-v_{2,i}^n\right)\mathrm{g}^{10}\left(x_{1,j}-x_{1,i},x_{2,j}-x_{2,i}\right)\end{array}\right)V_j\right) \\
-\rho_i^{n+1}\sum_{j=1}^{N_i}\left(v_{2,j}^n-v_{2,i}^n\right)\left(v_{1,i}^n\mathrm{g}^{10}\left(x_{1,j}-x_{1,i},x_{2,j}-x_{2,i}\right)+v_{2,i}^n\mathrm{g}^{01}\left(x_{1,j}-x_{1,i},x_{2,j}-x_{2,i}\right)\right)V_j
\end{array}\right)$$

$$+g_i^n \tag{52b}$$

where a_1 and a_2 are the acceleration components in x_1 and x_2 directions, respectively. The velocity is explicitly predicted by using the Forward Euler Method as

Velocity:

$$v_{1,i}^{n+1}=v_{1,i}^n+a_{1,i}^n\Delta t \tag{53a}$$

$$v_{2,i}^{n+1}=v_{2,i}^n+a_{2,i}^n\Delta t \tag{53b}$$

The displacement is predicted by using the Backward Euler Method as

Displacement:

$$u_{1,i}^{n+1} = u_{1,i}^{n} + v_{1,i}^{n+1}\Delta t \tag{54a}$$

$$u_{2,i}^{n+1} = u_{2,i}^{n} + v_{2,i}^{n+1}\Delta t \tag{54b}$$

Conservation of Energy:

$$T_i^{n+1} = T_i^n + \frac{\Delta t}{\rho_i^{n+1} C}\left(\begin{array}{l}
\left(\sum_{j=1}^{N_i}\left(k_j^n - k_i^n\right) g^{10}\left(x_{1,j} - x_{1,i}, x_{2,j} - x_{2,i}\right) V_j\right)\left(\sum_{j=1}^{N_i}\left(T_j^n - T_i^n\right) g^{10}\left(x_{1,j} - x_{1,i}, x_{2,j} - x_{2,i}\right) V_j\right) \\
+\left(\sum_{j=1}^{N_i}\left(k_j^n - k_i^n\right) g^{01}\left(x_{1,j} - x_{1,i}, x_{2,j} - x_{2,i}\right) V_j\right)\left(\sum_{j=1}^{N_i}\left(T_j^n - T_i^n\right) g^{01}\left(x_{1,j} - x_{1,i}, x_{2,j} - x_{2,i}\right) V_j\right) \\
+k_i^n \sum_{j=1}^{N_i}\left(T_j^n - T_i^n\right)\left(g^{20}\left(x_{1,j} - x_{1,i}, x_{2,j} - x_{2,i}\right) + g^{02}\left(x_{1,j} - x_{1,i}, x_{2,j} - x_{2,i}\right)\right) V_j \\
+\mu_i^n \left(\begin{array}{l}
2\left(\sum_{j=1}^{N_i}\left(v_{1,j}^n - v_{1,i}^n\right) g^{10}\left(x_{1,j} - x_{1,i}, x_{2,j} - x_{2,i}\right) V_j\right)^2 \\
+2\left(\sum_{j=1}^{N_i}\left(v_{2,j}^n - v_{2,i}^n\right) g^{01}\left(x_{1,j} - x_{1,i}, x_{2,j} - x_{2,i}\right) V_j\right)^2 \\
+\left(\sum_{j=1}^{N_i}\left(\begin{array}{l}\left(v_{1,j}^n - v_{1,i}^n\right) g^{01}\left(x_{1,j} - x_{1,i}, x_{2,j} - x_{2,i}\right) \\ +\left(v_{2,j}^n - v_{2,i}^n\right) g^{01}\left(x_{1,j} - x_{1,i}, x_{2,j} - x_{2,i}\right)\end{array}\right) V_j\right)^2
\end{array}\right) \\
-\rho_i^{n+1} C \sum_{j=1}^{N_i}\left(T_j^n - T_i^n\right)\left(\begin{array}{l} v_{1,i}^n g^{10}\left(x_{1,j} - x_{1,i}, x_{2,j} - x_{2,i}\right) \\ +v_{2,i}^n g^{01}\left(x_{1,j} - x_{1,i}, x_{2,j} - x_{2,i}\right)\end{array}\right) V_j + Q
\end{array}\right) \tag{55}$$

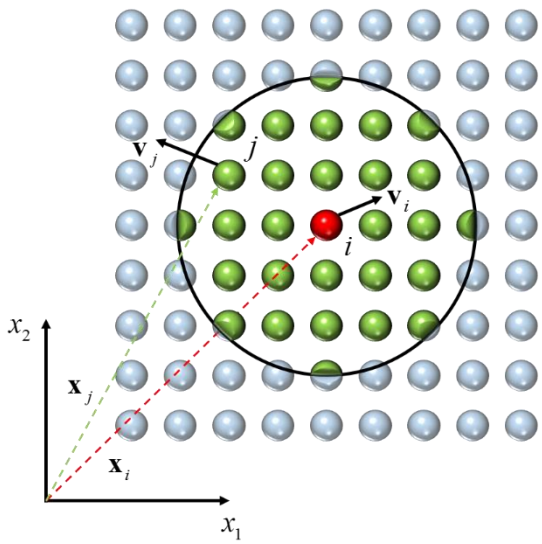

Fig. 2 PD discretization illustration: central point i and horizon $\delta = 3\Delta x$ with Δx being the point spacing distance

4.2 Boundary Conditions

The implementation boundary conditions can be adopted by using fictitious layers in PD theory [16, 18, 19, 23, 46-48]. The fictitious particles are fixed in the time integration. The thickness of the fictitious layer (shown by red spheres) is chosen as the size of the horizon shown in Fig. 3. Particle i represents the fictitious particle which is also considered as a central particle. Particle j which belongs to the fluid represents the family member of particle i.

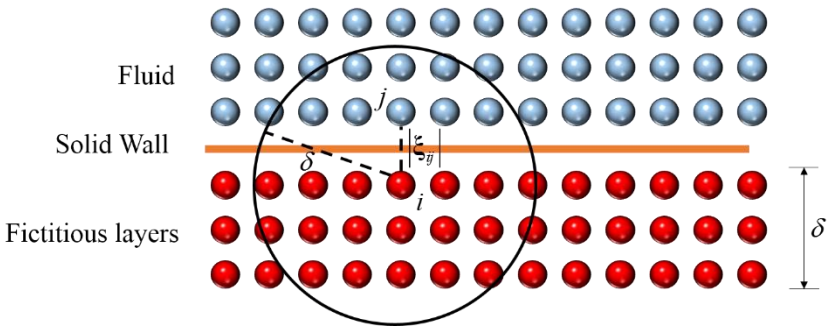

Fig. 3 Boundary implementation by using the fictitious layers

In the flow field, the acceleration, velocity, and displacement of particle i are defined according to the solid boundary condition as

$$\mathbf{a}_i = \mathbf{a}_{wall} \tag{56a}$$

$$\mathbf{v}_i = \mathbf{v}_{wall} \tag{56b}$$

$$\mathbf{u}_i = \mathbf{u}_{wall} \tag{56c}$$

The pressure is calculated according to the formulation provided in [49] as

$$p_i = \frac{\sum_{j=1} \left(p_j + \left(\mathbf{g} - \rho_j \mathbf{a}_i \right) \cdot \left(\mathbf{x}_j - \mathbf{x}_i \right) \right) w\left(\left| \boldsymbol{\xi}_{ij} \right| \right)}{\sum_{j=1} w\left(\left| \boldsymbol{\xi}_{ij} \right| \right)} \tag{57}$$

The weighted function $w\left(\left|\boldsymbol{\xi}_{ij}\right|\right)$ is provided in Eq.(12) with the definition of $\left|\boldsymbol{\xi}_{ij}\right|$ being shown in Fig. 3. According to Eq.(24), the density of the fictitious particle i is calculated as [45]

$$\rho_i = \frac{p_i}{c_s^2} + \rho_0 \tag{58}$$

The temperature on the boundary is denoted as T_{wall}. The temperature of the fictitious particle i is implemented as [18, 19, 47]

$$T_i = 2T_{wall} - T_j \tag{59}$$

The fictitious particles, j are located at the same distances from the boundary as the fluid particles, i as shown in Fig. 4

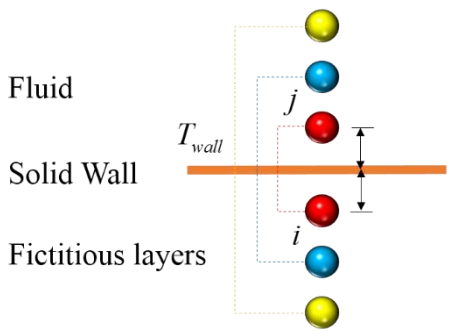

Fig. 4 Temperature boundary implementation (the pair of the fictitious particle and its corresponding fluid particle are shown in the same colour)

4.3 Numerical Algorithm

The flowchart of the numerical algorithm is provided in Fig. 5. Firstly, the peridynamic differential operator is constructed as a function of the initial relative position. Therefore, the construction of peridynamic differential operator is conducted prior to the time integration. The Math Kernel Library (MKL) [50] is adopted for solving Eq.(14) to obtain the peridynamic differential operators. Secondly, both the thermal and flow fields are considered in the program. Thus, a flag array is constructed to indicate the material points interactions belonging to the

thermal field or the flow field. Finally, the thermal field and the flow field are considered in a coupled manner.

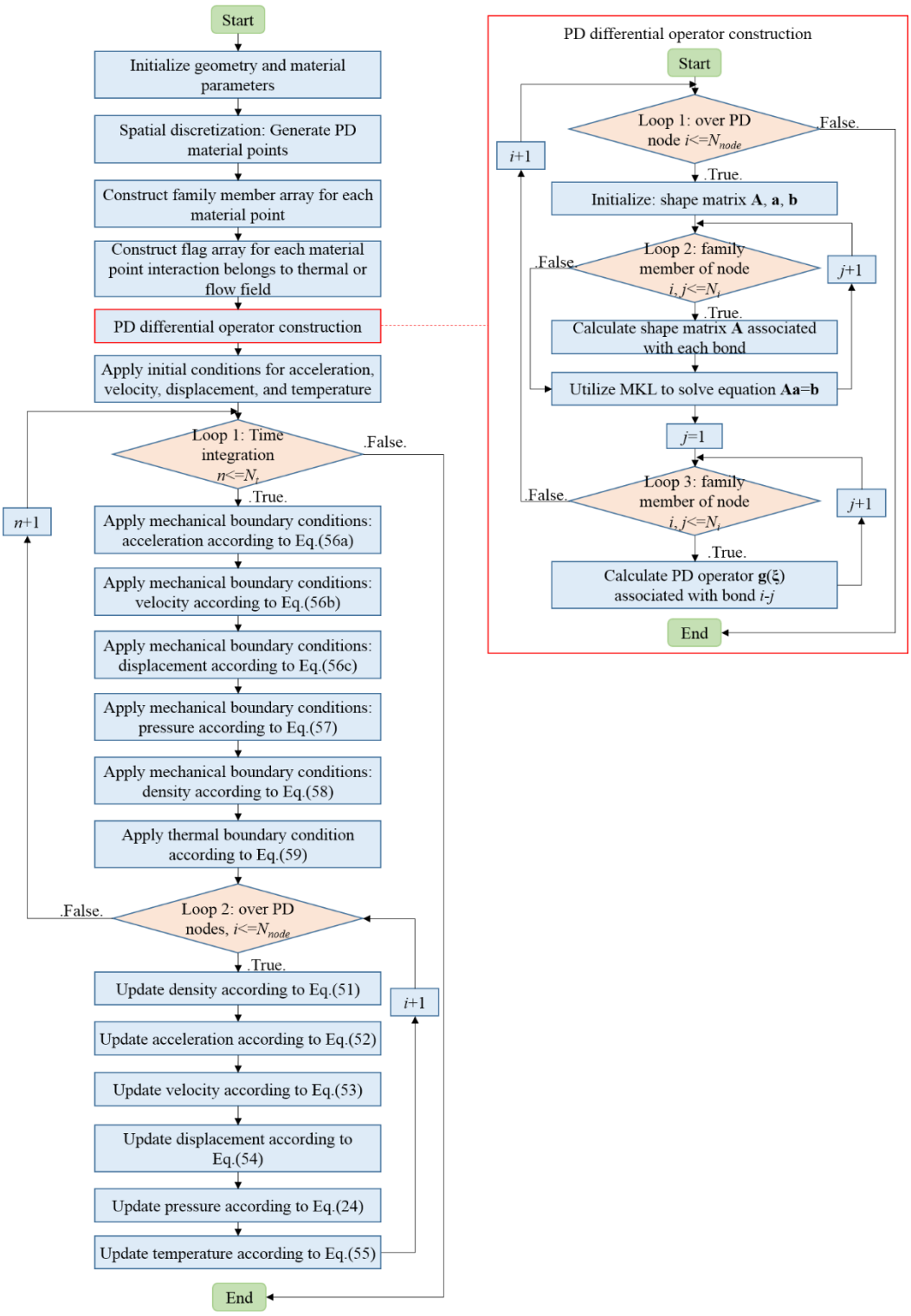

Fig. 5 Flowchart for numerical algorithm

5 NUMERICAL SIMULATIONS

In this section, three numerical simulations are conducted by applying the developed PD model. Firstly, heat conduction for a 2-D plate is conducted. The PD predicted results are compared with the solutions from ANSYS software. Secondly, natural convection in a cavity is simulated. Finally, mixed convection in a cavity is simulated. The predicted results from convection problems are compared with the ones from the previous literature.

5.1 Pure Heat Conduction Simulation

First, heat conduction in a 2-D plate is simulated. The length and width of the plate are $L = W = 0.1\,\mathrm{m}$. The thickness is $h = 0.001\,\mathrm{m}$. The material properties are set as: the thermal conductivity $k = 8.3075\,\mathrm{W/(mK)}$; the density $\rho = 1620\,\mathrm{kg/m^3}$; the specific heat capacity $c_v = 1092.728\,\mathrm{J/(kgK)}$. All the four boundaries are subjected to a constant temperature $T = 10\,\mathrm{K}$. The initial temperature is zero. Without considering the velocity and internal heat generation terms, the governing equation Eq. (32) with a constant thermal conductivity for heat conduction becomes

$$\rho c_v \frac{\partial T}{\partial t} = k \Delta T \tag{60}$$

For PD implementation, the mesh size for *x*-*y* plane is $\Delta x = 0.0005\,\mathrm{m}$. There is one layer in the thickness direction. The horizon is chosen as $\delta = 3.015\Delta x$. Similar to the derivation performed by Silling and Askari [39] and Oterkus et al. [18], a von Newman stability condition is applied. The stability condition of the present model for heat conduction problems is obtained as

$$\mathrm{d}t \le \rho c_v \Big/ \left(k \sum_{j=1}^{N} \left(g^{20}(\xi) + g^{02}(\xi) \right) V_j \right) \tag{61}$$

As a result, the time step size is chosen as $\mathrm{d}t = 0.01\,\mathrm{s}$. The total simulation time is 40s. The heat conduction is also simulated by using ANSYS software. The mesh size is chosen as $\Delta x = 0.001\,\mathrm{m}$ and the time step is $0.4\,\mathrm{s}$. The element type is chosen as PLANE55. The PD predicted temperature distribution is compared with ANSYS results as shown in Fig. 6. The good agreement validates the capability of the developed model for solving the pure two-dimensional heat transfer problem.

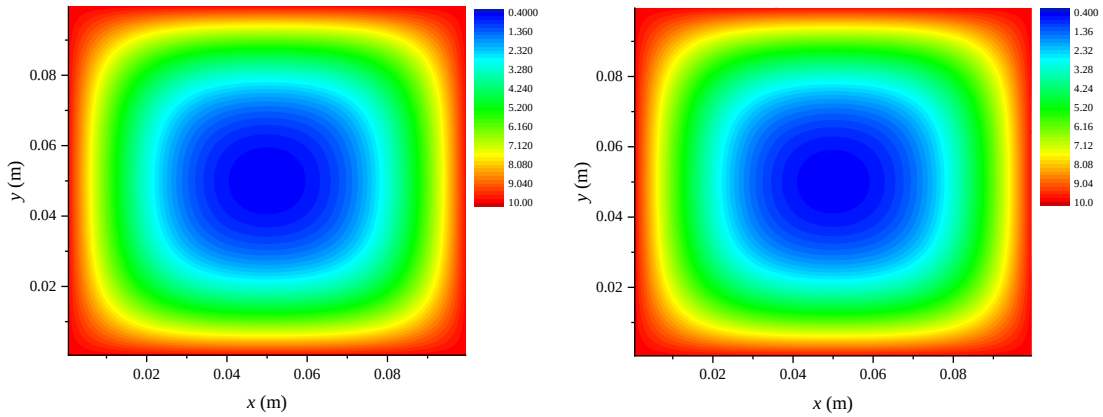

(a) (b)

Fig. 6 Temperature (K) distribution comparison between (a) ANSYS and (b) PD

5.2 Natural Convection in a Square Cavity

Second, a natural convection in a closed cavity is simulated in a non-dimensional form. A scheme of the two-dimensional natural convection problem, accompanying with the coordinate definitions and boundary conditions are shown in Fig. 7. For the initial state, the fluid is stationary and its temperature is zero. The boundary conditions are defined as

$$\text{at } x^* = 0: \ T^* = 1, \ v_1^* = v_2^* = 0 \tag{62a}$$

$$\text{at } x^* = 1: \ T^* = 0, \ v_1^* = v_2^* = 0 \tag{62b}$$

$$\text{at } y^* = 0: \ \partial T^* / \partial y^* = 0, \ v_1^* = v_2^* = 0 \tag{62c}$$

$$\text{at } y^* = 1: \ \partial T^* / \partial y^* = 0, \ v_1^* = v_2^* = 0 \tag{62d}$$

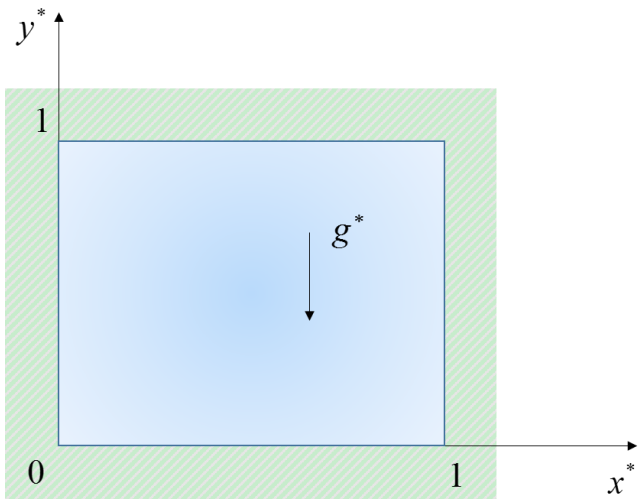

Fig. 7 Illustration for two-dimensional natural convection problem

For the natural convection in the cavity, the fluid flow is assumed to be weakly compressible. The fluid properties are assumed to be constant. Therefore, the viscous coefficient μ and the thermal conductivity k are uniform and constant for each PD point, i.e. $\mu = \mu_0; k = k_0$. The energy dissipation due to viscosity is neglected [6]. The Péclet number (Pe=RePr) is equal to 1 [6]. As a result, the non-dimensional parameters in Eq. (43) and Eq. (45) are

$$\mu^* = 1; k^* = 1; \mathrm{Ec} = 0; \mathrm{Re}\,\mathrm{Pr} = 1 \tag{63}$$

Furthermore, the Boussinesq approximation [51] is adopted. Hence, the value of non-dimensional gravity acceleration is approximated as

$$g^* = \mathrm{Ra}\,\mathrm{Pr}\,T^* \tag{64}$$

where Ra is the Rayleigh number defined as

$$\mathrm{Ra} = \frac{g\beta\Delta T L_0^3 \rho^2 C}{\mu k} \tag{65}$$

where β is the thermal expansion coefficient and ΔT is the temperature difference across the cavity.

Regarding the PD implementation, the mesh size is chosen as $\Delta x^* = 1/200$, and the horizon is chosen as $\delta^* = 3.015\Delta x^*$. The time step size is $\mathrm{d}t^* = 1\times10^{-5}$. The total simulation time is $t^* = 3$, leading to a steady state of the fluid flow at the end of the simulation. The

boundary implementation is illustrated in Fig. 8. Regarding the flow field, four fictitious layers are added to simulate the four solid walls. Their thicknesses are chosen as the size of the horizon. The accelerations, velocities, and displacements of the fictitious particles (shown in red colour) are zero. On the other hand, for the thermal field, two fictitious layers are added to implement the constant temperature boundary conditions. The temperature of the fictitious particle $\mathbf{x}'^*$ is set as [18]

$$T^*\left(x'^*, y^*, t^*\right) = 2 - T^*\left(x^*, y^*, t^*\right) \text{ for } x'^* + x^* = 0 \text{ and } y'^* = y^* \tag{66a}$$

$$T^*\left(x'^*, y^*, t^*\right) = -T^*\left(x^*, y^*, t^*\right) \text{ for } x'^* + x^* = 2 \text{ and } y'^* = y^* \tag{66b}$$

where $\mathbf{x}^*$ represents the corresponding fluid particle.

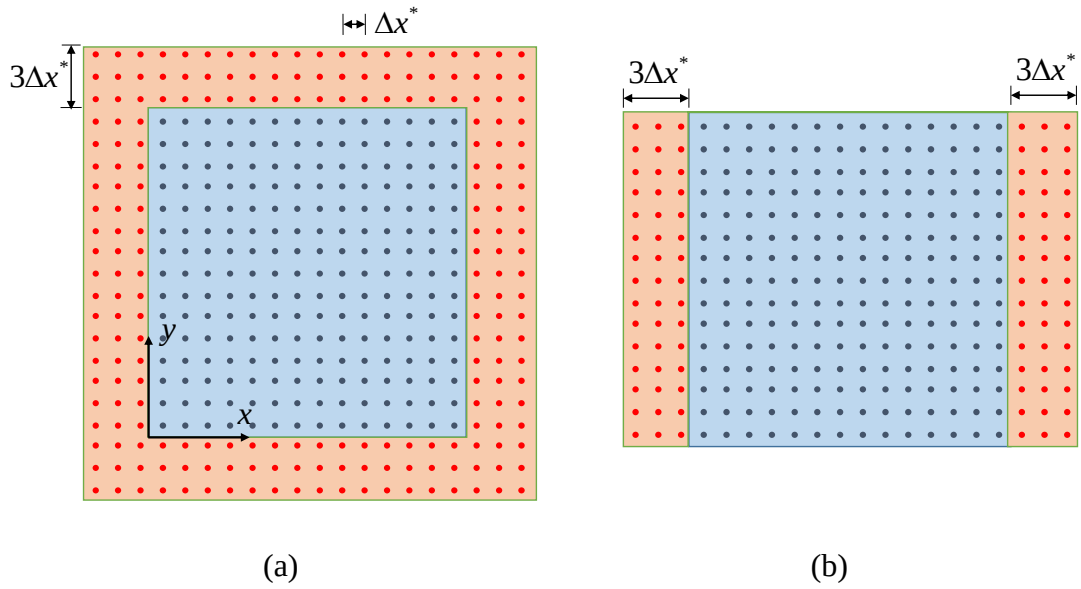

Fig. 8 Illustrations of PD discretization and boundary implementation for (a) flow field and (b) thermal field

There are three simulation cases considered. The non-dimensional numbers in the mathematical model are set as $\mathrm{Ra} = 10^3, 10^4, 10^5$ and $\mathrm{Pr} = 0.71$. The simulation results are compared with the ones from the published literature. Firstly, the flow velocity and temperature fields at the steady state are provided in Fig. 9 for $\mathrm{Ra}=10^3$, Fig. 10 for $\mathrm{Ra}=10^4$, and Fig. 11 for $\mathrm{Ra}=10^5$. The flow patterns and temperature distributions agree well with the solutions provided in [3, 5-7].

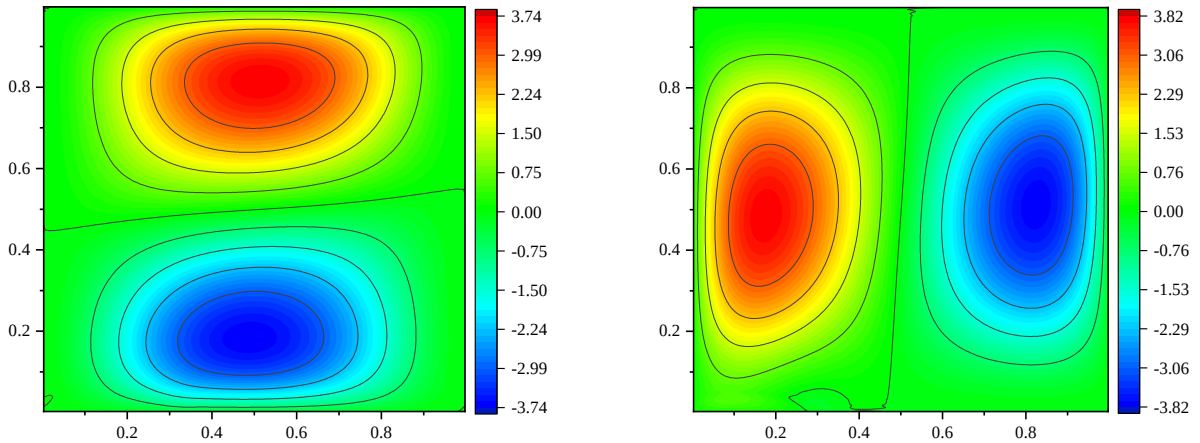

(a) (b)

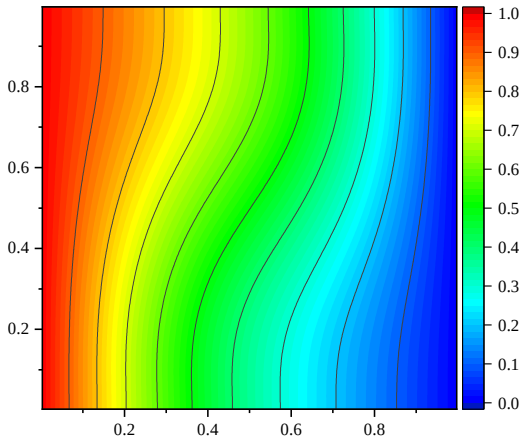

(c)

Fig. 9 Simulation results for Ra=10^3 and Pr=0.71: (a) horizontal velocity distribution, (b) vertical velocity distribution, and (c) temperature distribution

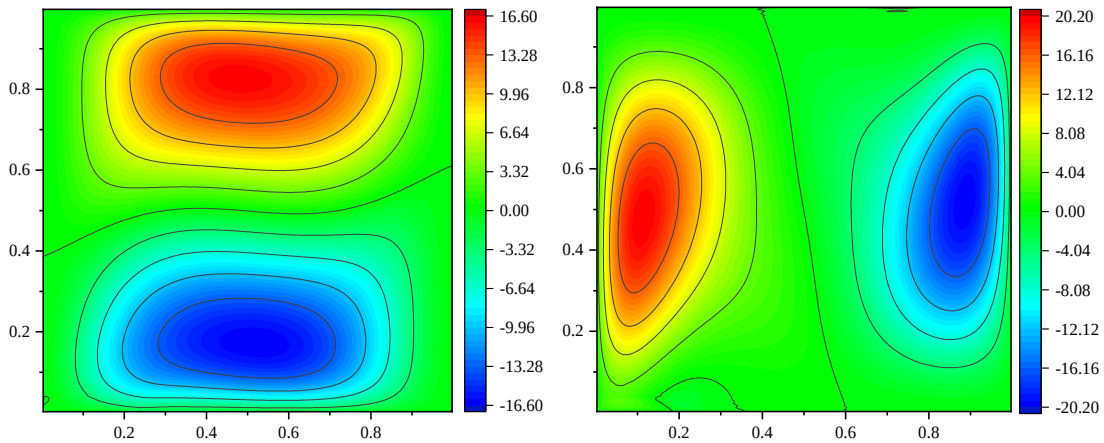

(a) (b)

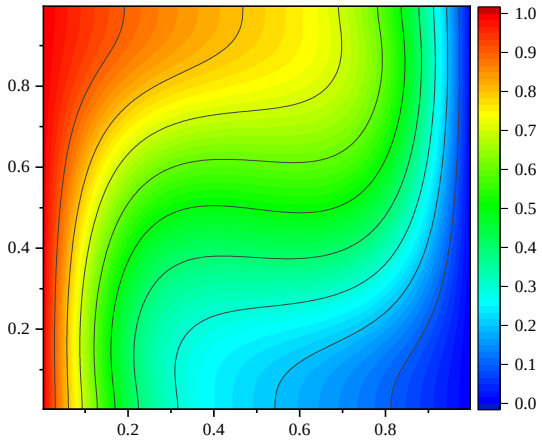

(c)

Fig. 10 Simulation results for Ra=10^4 and Pr=0.71: (a) horizontal velocity distribution, (b) vertical velocity distribution, and (c) temperature distribution

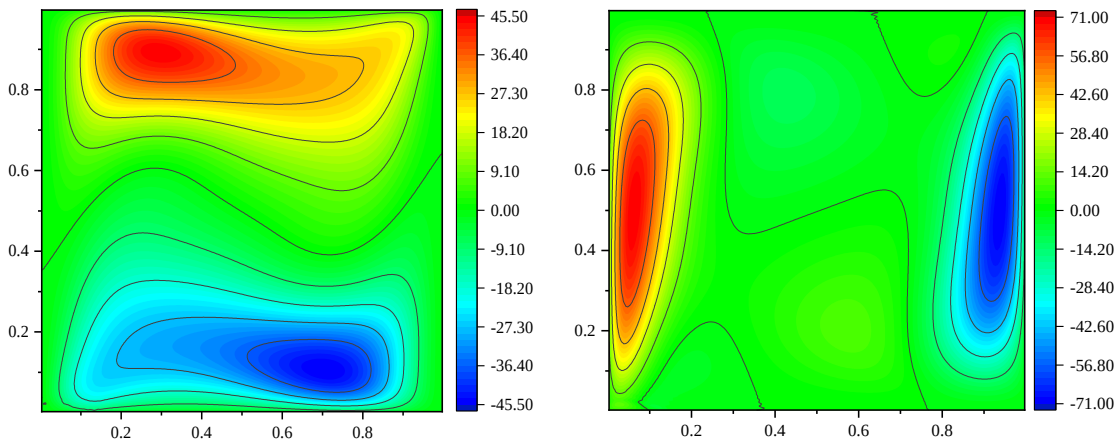

(a) (b)

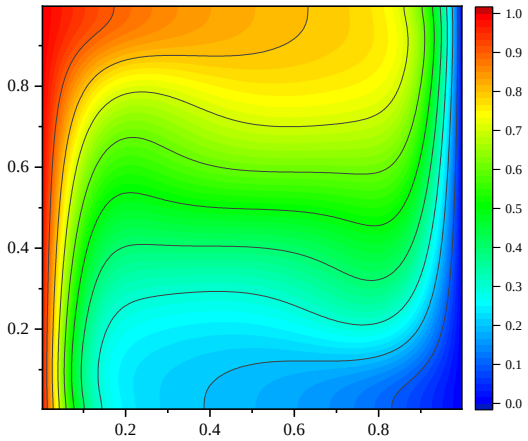

(c)

Fig. 11 Simulation results for Ra=10^5 and Pr=0.71: (a) horizontal velocity distribution, (b) vertical velocity distribution, and (c) temperature distribution

Later on, the profiles of horizontal velocity, vertical velocity, and temperature on the mid-plane are compared with the ones provided in [5] and [9], as shown in Fig. 12. In addition, the local Nusselt number along the hot wall ($x^* = 0$) is compared with the reference data provided in [9] obtained by ISPH, as shown in Fig. 13. It can be inferred from the figures that the PD predicted results agree well with the previous ones.

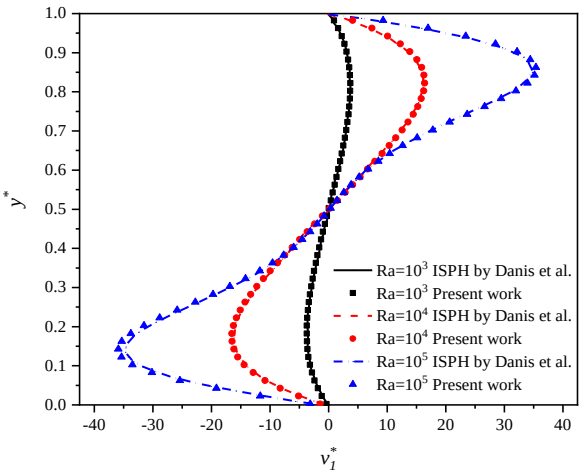

(a)

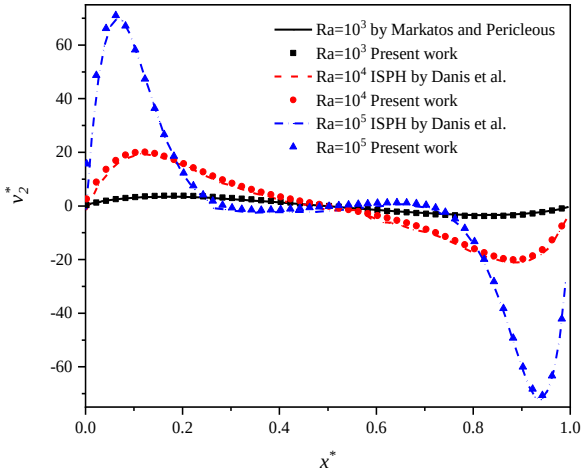

(b)

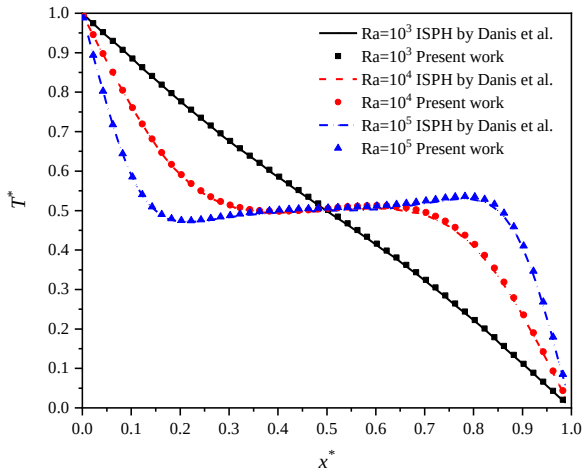

(c)

Fig. 12 Comparisons of dimensionless quantities (a) horizontal velocity on $x^* = 0.5$, (b) vertical velocity on $y^* = 0.5$, and (c) temperature on $y^* = 0.5$. Reference data is obtained by Danis et al. [9] and Markatos and Pericleous [5].

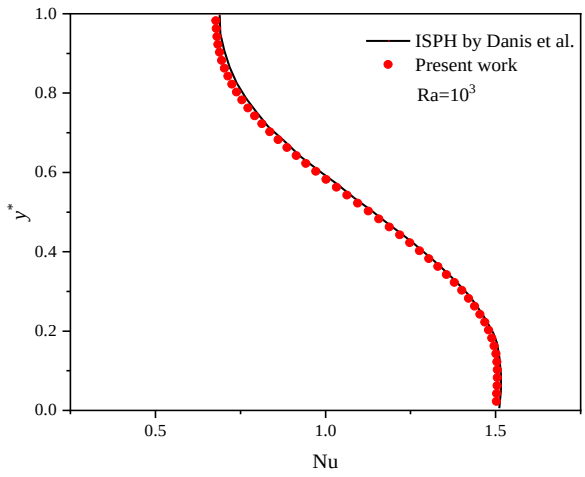

(a)

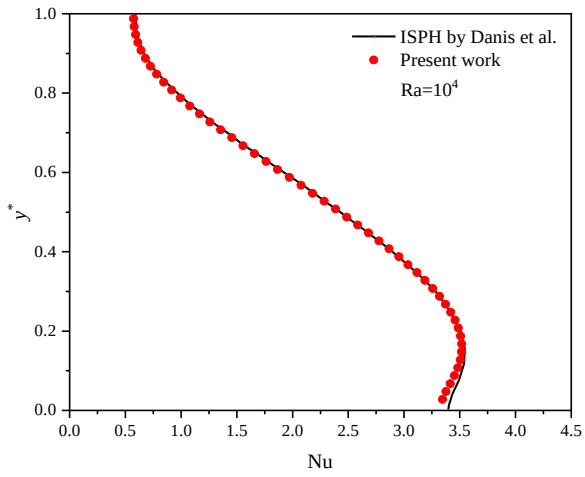

(b)

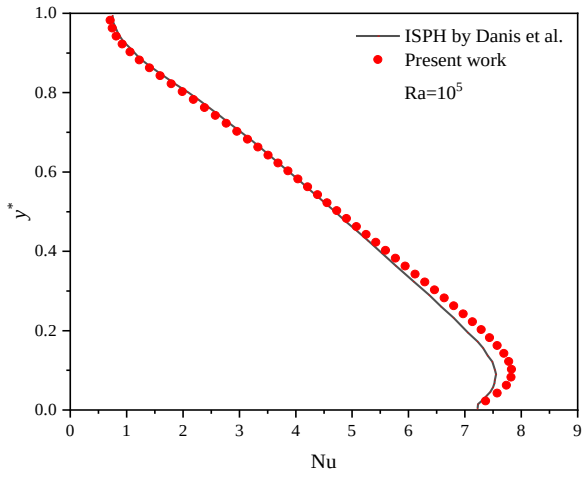

(c)

Fig. 13 Comparison of the local Nusselt number along with the hot wall ($x^* = 0$) for (a) Ra=10^3, (b) Ra=10^4, and (c) Ra=10^5. Reference data is from Danis et al. [9].

Finally, as a summary shown in Table 1, the representative quantities predicted by the PD model are compared with the available results obtained from finite difference method (FDM) [3], finite volume method (FVM) [5, 52], smoothed particle hydrodynamics (SPH) [8, 9], discrete singular convolution (DSC) [7].

Table 1 Comparison of the representative quantities.

	Present Work	[3]	[5]	[8]	[7]	[9]	[52]
Ra=10^3							
$v^*_{1,\max}$	3.731	3.649	3.544	3.431	3.643	3.666	4.077
$y^*_{\max}$	0.818	0.813	0.832	0.812	0.817	0.813	0.806
$v^*_{2,\max}$	3.796	3.697	3.593	3.511	3.686	3.720	4.130
$x^*_{\max}$	0.178	0.178	0.168	0.176	0.183	0.175	0.181
Nu_0	1.115	1.117	-	1.033	1.073	1.119	1.114
$\mathrm{Nu}_{\max}$	1.506	1.505	1.496	1.392	1.444	1.511	1.581
$\mathrm{Nu}_{\min}$	0.678	0.692	0.720	0.705	0.665	0.689	0.670
Ra=10^4							
$v^*_{1,\max}$	16.423	16.178	16.180	17.312	15.967	16.207	16.263
$y^*_{\max}$	0.828	0.823	0.832	0.823	0.817	0.825	0.818
$v^*_{2,\max}$	20.082	19.617	19.440	20.051	19.980	19.896	19.717
$x^*_{\max}$	0.118	0.119	0.113	0.112	0.117	0.113	0.119
Nu_0	2.253	2.238	-	2.081	2.155	2.257	2.245
$\mathrm{Nu}_{\max}$	3.519	3.528	3.482	3.448	3.441	3.543	3.539
$\mathrm{Nu}_{\min}$	0.574	0.586	0.643	0.541	0.528	0.584	0.583
Ra=10^5							
$v^*_{1,\max}$	35.441	34.730	35.730	-	33.510	34.745	35.173
$y^*_{\max}$	0.858	0.855	0.857	-	0.850	0.863	0.859
$v^*_{2,\max}$	70.987	68.59	69.08	-	70.81	70.448	69.746
$x^*_{\max}$	0.063	0.066	0.067	-	0.070	0.063	0.066
Nu_0	4.621	4.509	-	-	4.352	4.526	4.51
$\mathrm{Nu}_{\max}$	7.831	7.717	7.626	-	7.662	7.584	7.636
$\mathrm{Nu}_{\min}$	0.707	0.729	0.824	-	0.678	0.743	0.733

$v^*_{1,\max}$: the maximum horizontal velocity on the vertical mid-plane

$y^*_{\max}$: the corresponding vertical coordinate for the material point with $v^*_{1,\max}$

$v^*_{2,\max}$: the maximum vertical velocity on the horizontal mid-plane

$x^*_{\max}$: the corresponding horizontal coordinate for the material point with $v^*_{2,\max}$

Nu_0 : the average Nusselt number on the hot wall ($x^* = 0$)

$\mathrm{Nu}_{\max}$: the maximum value of the Nusselt number on the hot wall ($x^* = 0$)

$\mathrm{Nu}_{\min}$: the minimum value of the Nusselt number on the hot wall ($x^* = 0$)

From the comprehensive comparison between the present simulation results and the published literature, it can be concluded that the present model is able to accurately predict the two-dimensional natural convection problem in an enclosed square cavity for different values of Ra number.

5.3 Mixed Convection in a Square Cavity

Thirdly, the problem of a mixed convection in a lid-driven square cavity is simulated in a non-dimensional form. The geometry dimensions and the coordinate definition are same as Fig. 7. The fluid is motionless at the initial state. An initial linear temperature field in the vertical direction is defined as [53]

$$T^*\left(x^*, y^*, t^*\right) = y^* \tag{67}$$

The boundary conditions are defined as

On $x^* = 0$: $\partial T^*/\partial x^* = 0$, $v_1^* = v_2^* = 0$ (68a)

On $x^* = 1$: $\partial T^*/\partial x^* = 0$, $v_1^* = v_2^* = 0$ (68b)

On $y^* = 0$: $T^* = 0$, $v_1^* = v_2^* = 0$ (68c)

On $y^* = 1$: $T^* = 1$, $v_1^* = 1, v_2^* = 0$ (68d)

Being similar with the natural convection problem, for the mixed convection problem, the fluid properties are also assumed to be constant and the viscous dissipation is also neglected [11]. As a result, the non-dimensional parameters in Eq. (43) and Eq. (45) are

$$\mu^* = 1; k^* = 1; \mathrm{Ec} = 0 \tag{69}$$

Furthermore, the Boussinesq approximation [51] is also adopted. The non-dimensional gravity acceleration is approximated as

$$g^* = \frac{\mathrm{Gr}}{\mathrm{Re}^2} T^* = \mathrm{Ri} T^* \tag{70}$$

where Gr and Ri are the Grashof number and the Richardson number defined as

$$\mathrm{Gr} = \frac{\mathrm{Ra}}{\mathrm{Pr}}, \ \mathrm{Ri} = \frac{\mathrm{Gr}}{\mathrm{Re}^2} \tag{71}$$

For PD implementation, the mesh size is chosen as $\Delta x^* = 1/100$. The horizon is chosen as $\delta = 3.015\Delta x^*$. The time step size is $\mathrm{d}t^* = 1\times10^{-5}$ and the total simulation time is $t^* = 50$. The mixed convection problem reaches a steady state at the end of the simulation time. The boundary implementation approach is the same as the one in the natural convection simulation.

There are three simulation cases for the mixed convection problem. For all the cases, the Prandtl number and the Grashof number are fixed as $\mathrm{Pr} = 0.71$ and $\mathrm{Gr} = 100$. The Reynold number is set as $\mathrm{Re} = 10, 100, 400$ respectively. As a result, the Richardson number becomes $\mathrm{Ri} = 1, 0.01, 0.000625$ correspondingly. Therefore, by varying the Reynold number, the different Richardson numbers can be obtained.

In order to demonstrate the capability of the proposed model for solving the two-dimensional mixed convection in a square cavity problem, the steady solution for Re=400 (Ri =0.000625) is compared with the one provided by Iwastu et al. [53]. The velocity profile comparisons are presented in Fig. 14. In addition, the comparison of the temperature profiles and the local Nusselt number profiles are shown in Fig. 15. It can be inferred from the comparisons that the results agree well with the published literature [53], validating the present model.

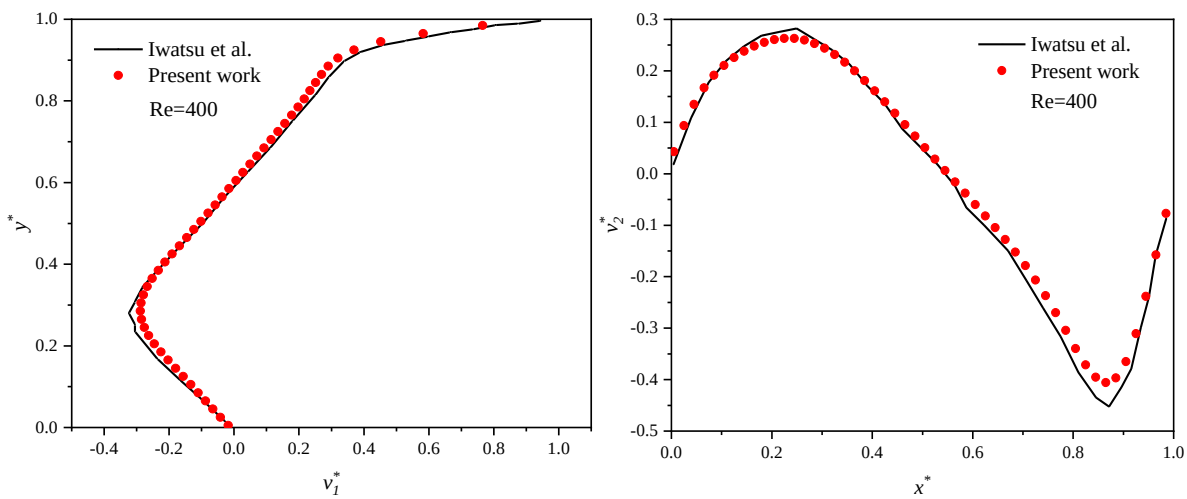

(a) (b)

Fig. 14 Comparison of velocity profiles for Re=400: (a) horizontal velocity on $x^* = 0.5$ and (b) vertical velocity on $y^* = 0.5$. Reference data is from Iwatsu et al. [53]

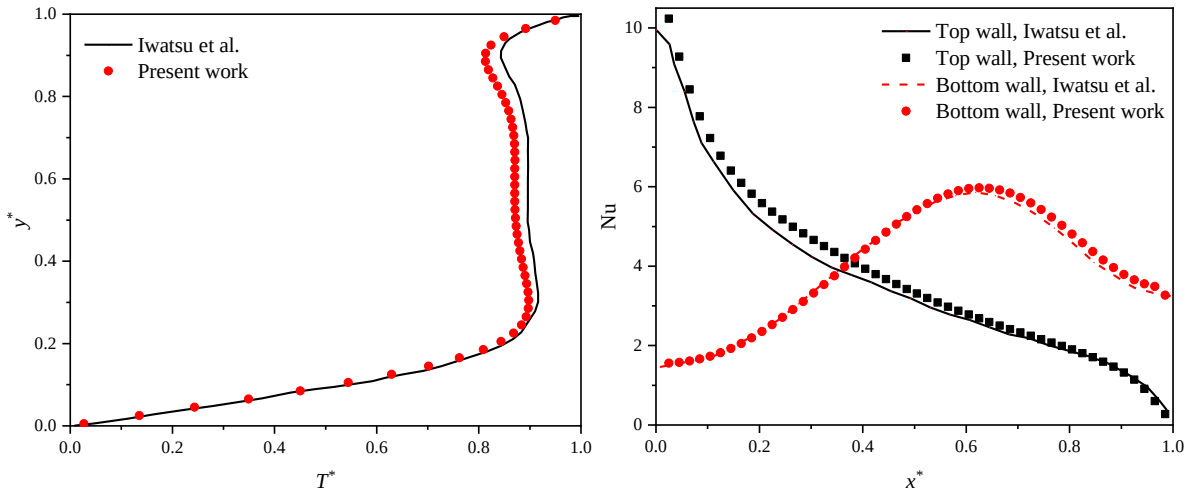

(a) (b)

Fig. 15 Comparison of thermal quantities for Re=400: (a) temperature profile on $x^* = 0.5$ and (b) local Nusselt profile at the top ($y^* = 1$) and bottom ($y^* = 0$) wall. Reference data is from Iwatsu et al. [53]

Later on, the average Nusselt numbers (Nu_{PD}) at the top wall of the cavity ($y^* = 1$) are provided in Table 2 for all the three cases. The comparison with Iwatsu et al. [53] Nu_{ref} is also provided. As it can be seen from Table 2, the relative error between the PD and reference results is less than 0.3%. The relative error is calculated as

$$\varepsilon_r = \frac{\left|\mathrm{Nu}_{PD} - \mathrm{Nu}_{ref}\right|}{\mathrm{Nu}_{ref}} \tag{72}$$

Table 2 Average Nusselt number at the top wall for all the three cases

Re	Ri	Present work Nu_{PD}	Iwatsu et al. [53] Nu_{ref}	ε_r
10	1	1.014	-	-
100	0.01	1.937	1.94	0.15%
400	0.000625	3.849	3.84	0.23%

Furthermore, the velocity and temperature profiles on the mid-plane are provided in Fig. 16. The temperature distributions are provided in Fig. 17 for the three cases.

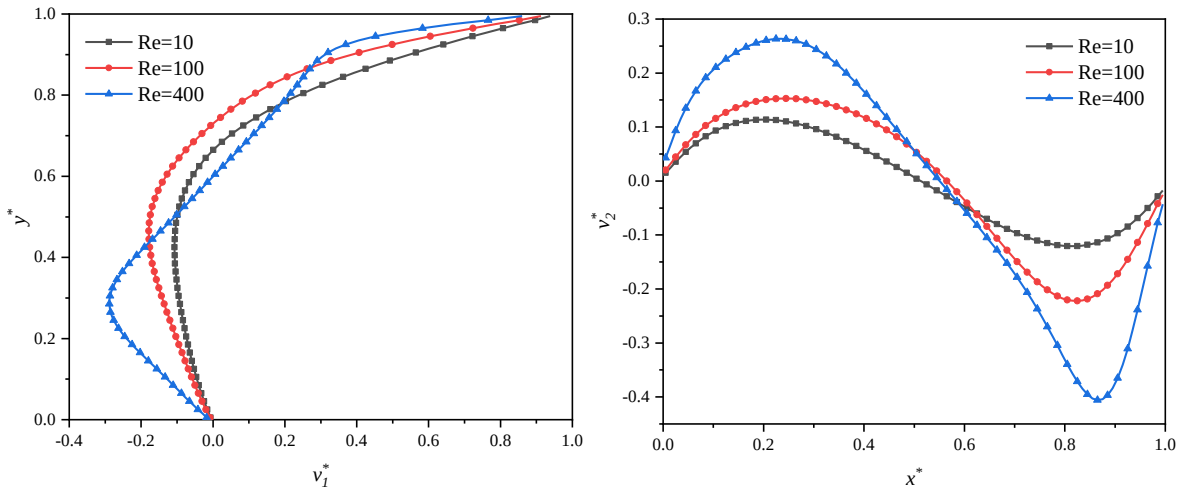

(a) (b)

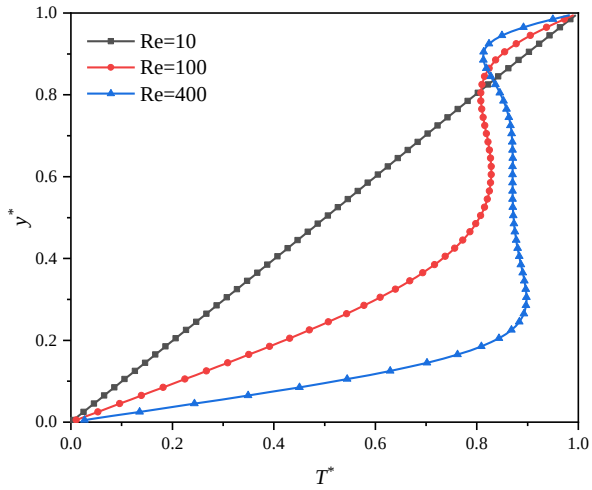

(c)

Fig. 16 Velocity and temperature profiles for all the three cases: (a) horizontal velocity on $x^* = 0.5$; (b) vertical velocity on $y^* = 0.5$; (c) temperature profile on $x^* = 0.5$.

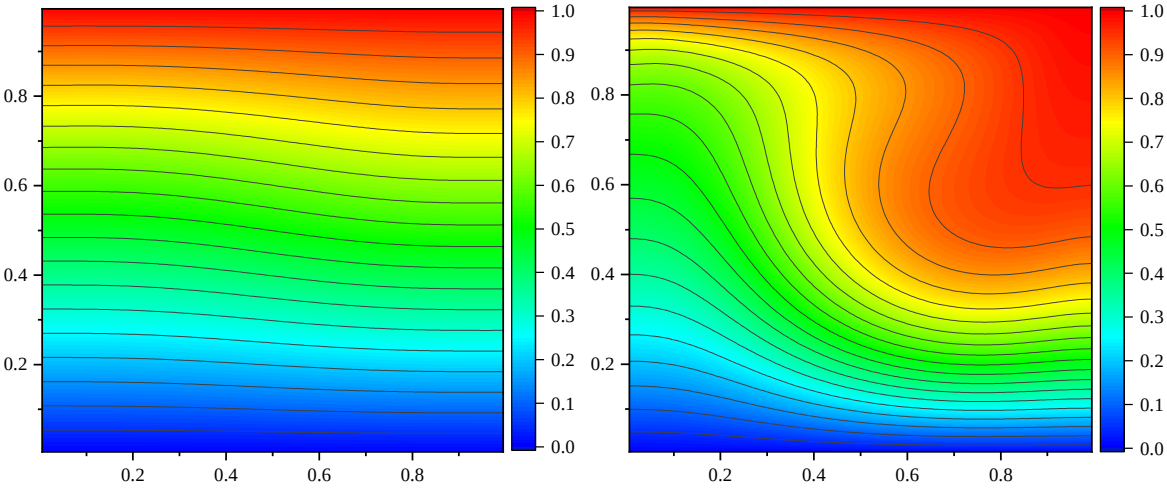

(a) (b)

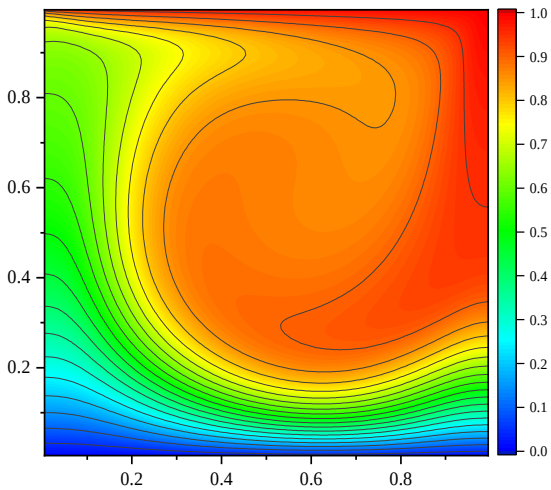

(c)

Fig. 17 Temperature field distribution for all the three cases: (a) Re=10, (b) Re=100, (c) Re=400

For a small value of Ri (Ri=0.000625 and Re=400 in this study), the fluid flow is dominated by the lid-driven force. The buoyancy effect is overwhelmed by the shear effect. For a low value of Ri (Ri=0.01 and Re=100 in this study), the buoyancy effect is comparable to the shear effect, leading to a mixed convection dominate situation. For an equivalent value of Ri (Ri=1 and Re=10 in this study), the buoyancy effect dominates the fluid flow, leading to a natural convection dominate simulation. The observations are consistent with the published literature [53, 54].

6 CONCLUSION

In this study, a coupled fluid flow and heat transfer model is developed by using the peridynamic differential operator. The classical spatial differential governing equations are converted into their non-local form. The developed model is applied to solve the pure heat conduction, the natural convection, and the mixed convection problems. The good match between the predicted results and the ones from the published literature validate the present model. The capability of the developed model for accurately simulating the coupled fluid flow and heat transfer phenomenon is thus demonstrated.

ACKNOWLEDGEMENTS

The authors gratefully acknowledge financial support from the China Scholarship Council (CSC No. 201506230126) and University of Strathclyde.

REFERENCES

[1] Corcione M. Effects of the thermal boundary conditions at the sidewalls upon natural convection in rectangular enclosures heated from below and cooled from above. Int J Therm Sci 2003;42(2): 199-208.
[2] Patankar S. Numerical heat transfer and fluid flow: CRC press; 1980.
[3] De Vahl Davis G. Natural convection of air in a square cavity: A bench mark numerical solution. Int J Numer Meth Fl 1983;3(3): 249-64.
[4] Elder JW. Turbulent Free Convection in a Vertical Slot. J Fluid Mech 1965;23(1): 99-111.
[5] Markatos NC, Pericleous KA. Laminar and Turbulent Natural-Convection in an Enclosed Cavity. Int J Heat Mass Tran 1984;27(5): 755-72.
[6] Szewc K, Pozorski J, Taniere A. Modeling of natural convection with Smoothed Particle Hydrodynamics: Non-Boussinesq formulation. Int J Heat Mass Tran 2011;54(23-24): 4807-16.
[7] C. Wan BP, GW Wei, D. A new benchmark quality solution for the buoyancy-driven cavity by discrete singular convolution. Numerical Heat Transfer: Part B: Fundamentals 2001;40(3): 199-228.
[8] Chaniotis AK, Poulikakos D, Koumoutsakos P. Remeshed smoothed particle hydrodynamics for the simulation of viscous and heat conducting flows. J Comput Phys 2002;182(1): 67-90.
[9] Danis ME, Orhan M, Ecder A. ISPH modelling of transient natural convection. Int J Comput Fluid D 2013;27(1): 15-31.
[10] Moallemi MK, Jang KS. Prandtl Number Effects on Laminar Mixed Convection Heat-Transfer in a Lid-Driven Cavity. Int J Heat Mass Tran 1992;35(8): 1881-92.
[11] Iwatsu R, Hyun JM, Kuwahara K. Mixed Convection in a Driven Cavity with a Stable Vertical Temperature-Gradient. Int J Heat Mass Tran 1993;36(6): 1601-08.
[12] Wong JCF. Numerical simulation of two - dimensional laminar mixed - convection in a lid - driven cavity using the mixed finite element consistent splitting scheme. Int J Numer Method H 2007;17(1): 46-93.
[13] Oztop HF, Dagtekin I. Mixed convection in two-sided lid-driven differentially heated square cavity. Int J Heat Mass Tran 2004;47(8-9): 1761-69.
[14] Sharif MAR. Laminar mixed convection in shallow inclined driven cavities with hot moving lid on top and cooled from bottom. Appl Therm Eng 2007;27(5-6): 1036-42.

[15] Silling SA. Reformulation of elasticity theory for discontinuities and long-range forces. J Mech Phys Solids 2000;48(1): 175-209.
[16] Madenci E, Oterkus E. Peridynamic theory and its applications: Springer; 2014.
[17] Oterkus E, Madenci E. Peridynamic Theory for Damage Initiation and Growth in Composite Laminate. Key Eng Mater 2012;488-489: 355-58.
[18] Oterkus S, Madenci E, Agwai A. Peridynamic thermal diffusion. J Comput Phys 2014;265: 71-96.
[19] Oterkus S, Madenci E, Agwai A. Fully coupled peridynamic thermomechanics. J Mech Phys Solids 2014;64: 1-23.
[20] Oterkus S. Peridynamics for the solution of multiphysics problems [Doctor of Philosophy]. Arizona: The University of Arizona; 2015.
[21] Bobaru F, Duangpanya M. A peridynamic formulation for transient heat conduction in bodies with evolving discontinuities. J Comput Phys 2012;231(7): 2764-85.
[22] Shojaei A, Galvanetto U, Rabczuk T, Jenabi A, Zaccariotto M. A generalized finite difference method based on the Peridynamic differential operator for the solution of problems in bounded and unbounded domains. Comput Method Appl M 2019;343: 100-26.
[23] Oterkus S, Madenci E. Peridynamic modeling of fuel pellet cracking. Eng Fract Mech 2017;176: 23-37.
[24] Oterkus S, Madenci E, Oterkus E, Hwang Y, Bae J, Han S. Hygro-thermo-mechanical analysis and failure prediction in electronic packages by using peridynamics. 2014 IEEE 64th Electronic Components and Technology Conference (ECTC)2014. 973-82.
[25] Oterkus S, Fox J, Madenci E. Simulation of electro-migration through peridynamics. 2013 IEEE 63rd Electronic Components and Technology Conference2013. 1488-93.
[26] Wang HL, Oterkus E, Oterkus S. Predicting fracture evolution during lithiation process using peridynamics. Eng Fract Mech 2018;192: 176-91.
[27] Madenci E, Oterkus S. Ordinary state-based peridynamics for thermoviscoelastic deformation. Eng Fract Mech 2017;175: 31-45.
[28] De Meo D, Oterkus E. Finite element implementation of a peridynamic pitting corrosion damage model. Ocean Eng 2017;135: 76-83.
[29] Diyaroglu C, Oterkus S, Oterkus E, Madenci E, Han S, Hwang Y. Peridynamic wetness approach for moisture concentration analysis in electronic packages. Microelectron Reliab 2017;70: 103-11.
[30] Han S, Lim S, Bae J, Hwang Y, Lee S, Oterkus S, et al. Equivalent acceleration assessment of JEDEC moisture sensitivity levels using peridynamics. 2015 IEEE 65th Electronic Components and Technology Conference (ECTC)2015. 1518-23.
[31] Gao Y, Oterkus S. Fully coupled thermomechanical analysis of laminated composites by using ordinary state based peridynamic theory. Compos Struct 2019;207: 397-424.
[32] Gao Y, Oterkus S. Ordinary state-based peridynamic modelling for fully coupled thermoelastic problems. Continuum Mech Therm 2018.
[33] Oterkus S, Madenci E, Oterkus E. Fully coupled poroelastic peridynamic formulation for fluid-filled fractures. Eng Geol 2017;225: 19-28.
[34] Wang J, Zhang X. Modified Particle Method with integral Navier–Stokes formulation for incompressible flows. J Comput Phys 2018;366: 1-13.
[35] Tu QS, Li SF. An updated Lagrangian particle hydrodynamics (ULPH) for Newtonian fluids. J Comput Phys 2017;348: 493-513.
[36] Silling SA, Parks ML, Kamm JR, Weckner O, Rassaian M. Modeling shockwaves and impact phenomena with Eulerian peridynamics. Int J Impact Eng 2017;107: 47-57.
[37] Ouchi H, Katiyar A, York J, Foster J, Sharma MM. A fully coupled porous flow and geomechanics model for fluid driven cracks: a peridynamics approach. Comput Mech 2015;55(3): 561-76.

[38] Madenci E, Barut A, Futch M. Peridynamic differential operator and its applications. Comput Method Appl M 2016;304: 408-51.
[39] Silling SA, Askari E. A meshfree method based on the peridynamic model of solid mechanics. Comput Struct 2005;83(17-18): 1526-35.
[40] Silling SA, Epton M, Weckner O, Xu J, Askari E. Peridynamic states and constitutive modeling. J Elasticity 2007;88(2): 151-84.
[41] Reddy JN, Gartling DK. The finite element method in heat transfer and fluid dynamics: CRC press; 2010.
[42] Morris JP, Fox PJ, Zhu Y. Modeling low Reynolds number incompressible flows using SPH. J Comput Phys 1997;136(1): 214-26.
[43] Liu G-R, Liu MB. Smoothed particle hydrodynamics: a meshfree particle method: World Scientific; 2003.
[44] Liu MB, Liu GR. Smoothed Particle Hydrodynamics (SPH): an Overview and Recent Developments. Arch Comput Method E 2010;17(1): 25-76.
[45] Batchelor GK. An introduction to fluid dynamics: Cambridge university press; 2000.
[46] Madenci E, Oterkus S. Peridynamics for Coupled Field Equations. Handbook of Peridynamic Modeling. New York: Chapman and Hall/CRC; 2016. 490-528.
[47] Oterkus S, Madenci E. Peridynamics for Antiplane Shear and Torsional Deformations. J Mech Mater Struct 2015;10(2): 167-93.
[48] Madenci E, Oterkus S. Ordinary state-based peridynamics for plastic deformation according to von Mises yield criteria with isotropic hardening. J Mech Phys Solids 2016;86: 192-219.
[49] Adami S, Hu XY, Adams NA. A generalized wall boundary condition for smoothed particle hydrodynamics. J Comput Phys 2012;231(21): 7057-75.
[50] Intel M. Intel math kernel library. 2007.
[51] Gray DD, Giorgini A. The validity of the boussinesq approximation for liquids and gases. Int J Heat Mass Tran 1976;19(5): 545-51.
[52] Barakos G, Mitsoulis E, Assimacopoulos D. Natural-Convection Flow in a Square Cavity Revisited - Laminar and Turbulent Models with Wall Functions. Int J Numer Meth Fl 1994;18(7): 695-719.
[53] Iwatsu R, Hyun JM, Kuwahara K. Mixed convection in a driven cavity with a stable vertical temperature gradient. Int J Heat Mass Tran 1993;36(6): 1601-08.
[54] Aly AM, Chamkha AJ, Lee SW, Al-Mudhaf AF. On Mixed Convection in an Inclined Lid-Driven Cavity with Sinusoidal Heated Walls Using the Isph Method. Comput Therm Sci 2016;8(4): 337-54.